Heliyon 10 (2024) e39139

Contents lists available at ScienceDirect

Heliyon

journal homepage: www.cell.com/heliyon

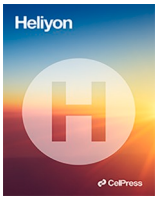

Research article

Maternal exposure to polystyrene nanoplastics induces sex-specific cardiotoxicity in offspring mice

Xiuli Chen [a], Shenzhen Huang [b,**], Li Wang [a], Kan Liu [a], Haiying Wu [a,*]

[a] Department of Gynecology and Obstetrics, Henan Provincial People's Hospital, People's Hospital of Zhengzhou University, School of Clinical Medicine of Henan University, Zhengzhou, Henan, 450003, China
[b] Henan Eye Institute, Henan Provincial People's Hospital, People's Hospital of Henan University, People's Hospital of Zhengzhou University, Zhengzhou, Henan, 450003, China

ARTICLE INFO

Keywords:
Offspring
Polystyrene nanoplastics
RNA-Seq
Heart
Sex-specific

ABSTRACT

Globally, plastic pollution threatens human health, particularly affecting the hearts of offspring exposed to maternal environmental factors early in development. Few studies have specifically addressed sex-specific cardiac injury in offspring resulting from maternal exposure to polystyrene nanoplastics (PS-NPs). This study investigates the potential cardiac injury in offspring following maternal exposure to 1 mg/L PS-NPs. Pregnant C57BL/6J mice were exposed to PS-NPs until 3 weeks postpartum to establish a maternal exposure model. Heart tissues were collected and weighed, and the transcriptomes of the offspring hearts were sequenced and analyzed using high-throughput RNA sequencing. Immunohistochemical staining was performed to assess the effects of PS-NPs on cardiac immune infiltration, fibrosis, and apoptosis in the offspring. PS-NPs caused a significant reduction in heart and body weight in female offspring compared to males. Additionally, PS-NPs induced sex-specific transcriptional reprogramming and metabolic disruptions in the offspring. PS-NPs also induced significant fibrosis, apoptosis, and increased $CD68^{+}$ macrophage infiltration in offspring hearts. Notably, PS-NPs induced distinct cardiovascular diseases in the offspring. Fluid shear stress and atherosclerosis were significantly enriched in PS-NP-treated male offspring, while viral myocarditis was predominantly enriched in PS-NP-treated females. Our findings suggest that PS-NPs induce cardiotoxicity in offspring by disrupting metabolism, impairing immunity, and triggering fibrosis and apoptosis, with sex-specific differences. This study provides novel insights and a foundation for understanding sex-specific pharmacological differences and interventions in PS-NP-induced cardiovascular disease in offspring.

1. Introduction

Plastic pollution poses a significant threat to human health, attracting widespread attention from researchers. Traces of plastic debris have been detected in human placenta [1], faeces [2], blood [3], breast milk [4], and organs such as the liver [5] and lungs [6]. By 2025, an estimated 11.0 billion tons of plastic will have accumulated in the environment [7], potentially excluding single-use plastics produced during COVID-19 pandemic [8]. Environmental plastic debris undergoes chemical and physical processes, breaking down into microplastics (<5 mm) or nanoplastics (NPs, <100 nm) [9–11]. As NPs proliferate, they increasingly enter the

* Corresponding author. Department of Gynecology and Obstetrics, Henan Provincial People's Hospital, Zhengzhou, Henan, 450003, China.
** Corresponding author. Henan Eye Institute, Henan Provincial People's Hospital, Zhengzhou, Henan, 450003, China.
E-mail addresses: huangshenzhen@zzu.edu.cn (S. Huang), wuhaiying@zzu.edu.cn (H. Wu).

https://doi.org/10.1016/j.heliyon.2024.e39139
Received 12 March 2024; Received in revised form 19 September 2024; Accepted 8 October 2024
Available online 11 October 2024
2405-8440/© 2024 The Authors. Published by Elsevier Ltd. This is an open access article under the CC BY-NC-ND license (http://creativecommons.org/licenses/by-nc-nd/4.0/).

human body through inhalation, ingestion, and dermal penetration [12]. Additionally, nanocarriers, including drugs and biomolecules (e.g., proteins, peptides), may be introduced into the body via injection [13]. NPs can even penetrate deeper into human tissues, posing a significant threat to health [14,15].

Currently, polystyrene nanoplastics (PS-NPs) are among the most widely available and studied nanomaterials [16–19]. PS-NPs can cross the blood-brain barrier, significantly impairing mouse neurons, as demonstrated by Shan et al. [20]. Additionally, He et al. [21] demonstrated that PS-NPs exacerbate LPS-induced duodenal inflammation in mice via the ROS-driven NF-κB/NLRP3 pathway. Chronic exposure to PS-NPs has been shown to exacerbate cardiotoxicity in mice, evidenced by myocardial fibrosis and autophagy [22]. Notably, PS-NP exposure during pregnancy and lactation induces toxicity in the liver and testes of male offspring in mice [23]. Pregnancy is a critical period for early-life growth and development, warranting careful consideration of the health risks posed by PS-NP exposure.

Adverse factors during early life, such as maternal nutrition, illness, as well as environmental exposures, can impact fetal development [24–26]. Previous studies suggest that NPs can penetrate various animal organs, including cell membranes, the blood-brain barrier, and the placenta, and can be transmitted to the next generation [27,28]. Tanwar et al. [29] demonstrated that in utero exposure to PM2.5 impaired cardiac performance in newborn mice by reducing left ventricular end-diastolic volume. Hathaway et al. [30] reported that maternal exposure to TiO_2 nanoparticles during pregnancy is associated with reduced cardiac function and diminished cardiomyocyte activity in rats. Additionally, PS-NP exposure in human blastocysts inhibits the development of atrioventricular heart valves in newborns [31]. NPs have also been shown to penetrate the placental barrier in rodents, transferring from mother to fetus and adversely affecting the fetal heart and other organs [32]. However, the mechanisms by which maternal PS-NP exposure damages fetal and infant heart tissue, leading to cardiovascular disease, remain poorly understood. Transcriptomic sequencing (RNA-seq) has emerged as a powerful tool for investigating changes in gene expression, offering a novel approach to identifying specific biological processes and underlying mechanisms [33].

To investigate the effects of PS-NPs on heart tissue in mouse offspring, a maternal exposure model was established by administering 1 mg/L PS-NPs in the drinking water of pregnant C57BL/6J mice, following previously reported protocols [34,35]. PS-NPs induced sex-specific cardiotoxicity by promoting fibrosis, apoptosis, increased $CD68^+$ macrophage infiltration, and metabolic disruption in the hearts of offspring. They also contributed to sexually dimorphic cardiovascular disease. In summary, this study demonstrates that maternal PS-NP exposure leads to sex-specific cardiotoxicity in offspring and offers a novel perspective on the underlying molecular mechanisms. These findings are crucial for developing therapeutic interventions targeting cardiovascular diseases induced by PS-NPs.

2. Material and methods

2.1. Materials

In this research, an aqueous suspension of PS-NPs (Cat # 43302, a particle size of 100 nm) was purchased from Sigma-Aldrich (Merck KGaA, USA). The stock solution was sonicated for 30 min to achieve uniform dispersion, then diluted with deionized water to a concentration of 1 mg/L for subsequent experiments.

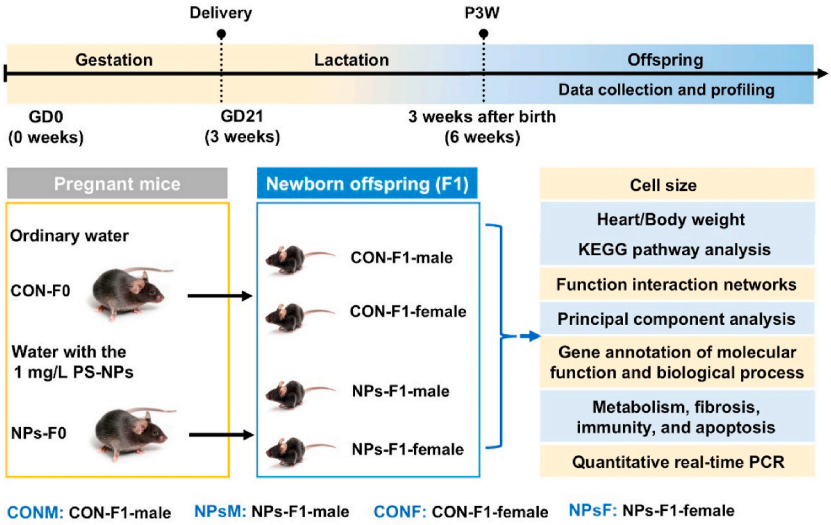

Fig. 1. Schematic of the experimental procedure.

2.2. Animals and PS-NPs exposure

Eighteen C57BL/6J wild-type mice, aged six to eight weeks old, were obtained from GemPharmatech Co., Ltd. (Nanjing, Jiangsu), consisting of six males and twelve females. Before the experiment began, the mice were acclimated for two weeks to a 12-h light/12-h dark cycle, with illumination from 7:00 a.m. to 7:00 p.m. Daily mating was then conducted at 7:00 p.m., with a female-to-male ratio of 2:1. During the mating period, the mice were provided with standard water and diet. The mice were examined for the presence of a white conical pessary in the vagina (a marker of successful conception) by a seasoned technician at 8:00 a.m. the following day. Female mice with poorly formed or misplaced vaginal plugs were excluded from the study. After mating, the males were removed. The 0th day of gestation (GD0) was defined as the day of the discovery of the vaginal plug. Subsequently, the pregnant mice were randomized into two groups: the non-PS-NPs-treated group (CON-F0) and the PS-NPs-treated group (NPs-F0). Each group consisted of five mice, with no significant difference in average body weight observed. During the experiment, both groups of mice were given a standard diet, but the water differed. Control mice received standard water, while experimental mice were given water containing 1 mg/L PS-NPs during gestation. At three weeks of age, the pups were weaned and provided with standard water until the end of the experiment. A concentration of 1 mg/L is typically used in such studies as it approximates environmental exposure levels [34–37]. Offspring were permitted free movement and had constant access to food and water. Bedding was changed weekly. The study utilized male and female offspring at three weeks of age for cardiac transcriptome sequencing (RNA sequencing, RNA-Seq) and additional analyses, including HE staining, masson staining, quantitative real-time PCR, and immunohistochemistry. Offspring were categorized as follows: male in the control group (CON-F1-male, namely CONM), male in the PS-NPs group (NPs-F1-male, namely NPsM), female in the normal group (CON-F1-female, namely CONF), and female in the PS-NPs group (NPs-F1-female, namely NPsF). Gene expression profiles related to metabolism, fibrosis, immunity, and apoptosis were analyzed using KEGG pathway analysis, functional interaction networks, and principal component analysis. Immunohistochemical staining was performed to assess the impact of PS-NPs on cardiac immune infiltration, fibrosis, and apoptosis in the offspring. The overall study design is illustrated in Fig. 1. All experimental protocols were approved by the Institutional Animal Care and Use Committee of Henan Provincial People's Hospital under ethics number (2021) Review No. 38.

2.3. Tissue collection

Upon death from cervical spine luxation, heart tissues from the CONM, NPsM, CONF, and NPsF groups were immediately excised and weighed. The tissues were stored in a freezer kept at −80 °C until later usage.

2.4. RNA extraction and RNA sequencing

To obtain macroscopic heart tissue devoid of free of fatty infiltrates, fibrosis, and blood, mouse heart tissue from the CONM, NPsM, CONF, and NPsF groups were collected, frozen, and subsequently crushed. RNA extraction was carried out according to the TRIzol RNA extraction protocol. The RNA Easy Spin Column Kit was purchased from Qiagen (Hilden, Germany). RNA libraries were generated using the DNBSEQ platform method, as previously reported [38,39]. The following is a brief description of the library preparation process. First, oligo-dT-tagged magnetic beads were employed to isolate poly(A)-tailed mRNA molecules from the total RNA sample. Next, the RNA was cleaved using disrupt buffer, transcribed with a random N6 primer, and the cDNA strands were synthesized into double-stranded DNA. Subsequently, the repaired complementary DNA and cDNA were purified, and double-stranded cDNA with the probe attached was isolated. Finally, specific primers were employed to amplify the ligation product via PCR. The PCR product was subjected to thermal denaturation, and circularization of the single-stranded DNA was achieved using a bridging primer to generate a single-stranded circular DNA library. RNA extraction and sequencing were conducted by the Beijing Genomic Institute (BGI) (Shenzhen, China). It is noteworthy that the reference genome used in this study was *Mus musculus*, obtained from NCBI.

2.5. Principal component analysis

Principal component analysis (PCA) is applied to summarize and visualize information in datasets containing individual or observational analyses with multiple interrelated variables [40]. Commonly, PCA calculations were performed to assess the quality of the RNA-seq. In this study, PCA was utilized to assess the overall similarity or differences in gene expression values of cardiac transcripts between the control group (CONM and CONF) and the PS-NPs group (NPsM and NPsF). PCA were shown by using Statistical Analysis of Metagenomic Profiles (STAMP) software.

2.6. Differentially expressed genes

Differentially expressed genes (DEGs) analysis is the statistical analysis of gene expression data under different treatments with the control group to screen out gene sets with significant expression changes [41]. The threshold criterion for statistically meaningful DEGs has been set at the following levels: $|\log2FC|$ was set as ≥ 1 and Q was set as < 0.05. After setting the significance threshold, the scatter plot is generated. Additionally, pie charts were created based on variations in gene expression levels of fragments per kilobase million (FPKM), sorted as low expression of genes: $0 <$ FPKM < 1, higher expression of genes: $1 \leq$ FPKM < 20, and highly expressed of genes FPKM ≥ 20 [42,43].

2.7. Quantitative real-time PCR

Total RNA was isolated from heart tissues as previously described [44–46]. The RNA was extracted using TRIzol reagent according to the manufacturer's protocol (Hilden, Germany) and subsequently subjected to cDNA synthesis using a PrimeScript RT-PCR kit (TAKARA Korea, Seoul, Korea). RT-PCR analysis was conducted using the SYBR mix and a CFX384 real-time system (Bio-Rad, Hercules, CA, USA). β-actin mRNA levels were used as internal controls for normalization. The primer sequences used are provided in Table S1.

2.8. Functional enrichment GO and KEGG analysis

The Kyoto Encyclopedia of Genes and Genomes (KEGG), a database for systematic study of the function of genes and genomic data, helping investigators study information on genes and their expression as a network. In the literature of other reports, pathways were defined as significantly enriched for DEGs when the *P*-value <0.05. But, in the study, with $Q < 0.05$ as the cut-off criterion, the *P*-value has been calculated using the Bonferroni correction [47]. The KEGG was carried out using BLASTALL software (Bethesda, United States) against the KEGG database version 81.0 and the NCBI RefSeq as the reference gene set (GCF_000001635.25_GRCm38.p5). Important relationships of candidate genes are obtained using gene ontology (GO) analysis, DEGs were submitted to analyze the molecular functions (GO-F) and biological processes (GO-P). The number of genes for each term is first calculated by mapping all the candidate genes to each term in the GO database. The importance of the biological functions of the screened genes was then determined using the hypergeometric test. GO terms which meet this requirement, (both $p < 0.05$ and false discovery rate (FDR) < 0.05), were considered to be an indication of statistical significance.

2.9. Protein-protein association networks

Protein-protein association networks (PPANs) were explained using version 11.5 of the STRING database [48]. Here, it is mainly used to reveal PPANs of metabolism, immunity, fibrosis, and apoptosis-related genes. The type of network was set to be a full STRING network. Experiments and databases were chosen as the sources of interactions. And, the STRING networks were clustered using k-means clustering.

2.10. Immunohistochemistry

Immunohistochemistry (IHC) utilizes the principle of exact binding between antigens and antibodies to locate antigens (peptides and proteins) in tissue cells [49]. A chemical reaction then ensues, leading to the chromogenic labeling of antibodies via agents such as enzymes, metal ions, fluorescein, and isotopes. The heart tissues of CONM, NPsM, CONF, and NPsF were paraffin-embedded. Experiments were performed following the procedures already reported in the literature to obtain the results. Paraffinized samples are dewaxed and hydration. Sections of mouse heart were immersed in xylene for 15–20 min, followed by rinsing with 75–100 % ethanol water. Among them, reagents xylene I-III and ethanol were purchased from Sinopharm Chemical Reagent Co., Ltd. (Shanghai, China). Next, the samples were closed and antigen repair. All antibodies, PBS, DAB, and hematoxylin stains used in the experiments were purchased from the Servicebio Company (Wuhan, China). Sections of mouse heart were placed on PBS after incubation in hydrogen peroxide solution (3 %). Then, block endogenous peroxidase. Anti-CD68 and antic-leaved caspase-3 antibody was incubated overnight with the heart section. After the heart sections were washed with PBS, secondary antibody was added, and then DAB color developing solution was added for culture, and hematoxylin was stained for 50 s. Finally, a series of operations such as dehydration, transparency, and drying are carried out before subsequent data reading. The heart sections were examined, imaged, and analyzed using a Pannoramic 250/MIDI light microscope (Hungary). Twenty 400X field images were chosen, positive cells were calculated in a double-blind fashion to quantify the infiltration and apoptosis of CD68 macrophages. And, apply version 1.53k of ImageJ software of Wayne Rasband (United States) to calculate the total number of cells.

2.11. Masson staining

Masson's trichrome staining is a staining method for collagen fibers and muscle fibers that can be used to observe the collagen structure in tissues and pathological tissues [50]. And it was carried out in accordance with a study that had already published. All heart sections from the CONM, NPsM, CONF, and NPsF groups were put into xylene I-III for 15–20 min, followed by sequential washing with 75–100 % ethanol and then rinsing with distilled water. Masson's trichrome staining kit purchased from Service Bio (G1006, Wuhan, China) was used to give heart slice staining, according to the recommendations of manufacturer. Cardiac sections were examined, imaged, and analyzed using a microscope. Twenty images at 400× magnification were randomly selected, and the area of the fibrotic tissue was counted in a double-blind fashion to calculate the degree of fibrosis. ImageJ software (same as above) was also used to obtain the ratio of the area of fibrotic tissue.

2.12. Hematoxylin-eosin staining

Hematoxylin-eosin (HE) staining was performed according to previously reported procedures in the literature [51]. Heart sections were then imaged and analyzed using the same light microscope. Twenty images at 400× magnification were randomly selected, and

ImageJ software was used to measure cardiac cell size.

2.13. Statistical analysis

The version 2.1.0 of the Venn diagram plotter (Venny) was applied to compare the transcript counts between the normal group and PS-NPs-treated group. The heatmap package in R (version 3.5.3) was used to visualize the expression of normal and PS-NPs group transcripts. The version 8.1.0 of GraphPad Prism software (La Jolla, CA, USA) was applied to charting and scatter plotting. STAMP statistical software was used for PCA. A 2-way analysis of variance (ANOVA) was adopted. The data were showed as the mean ± SEM (standard error) and were supposed statistically significant with the $P < 0.05$.

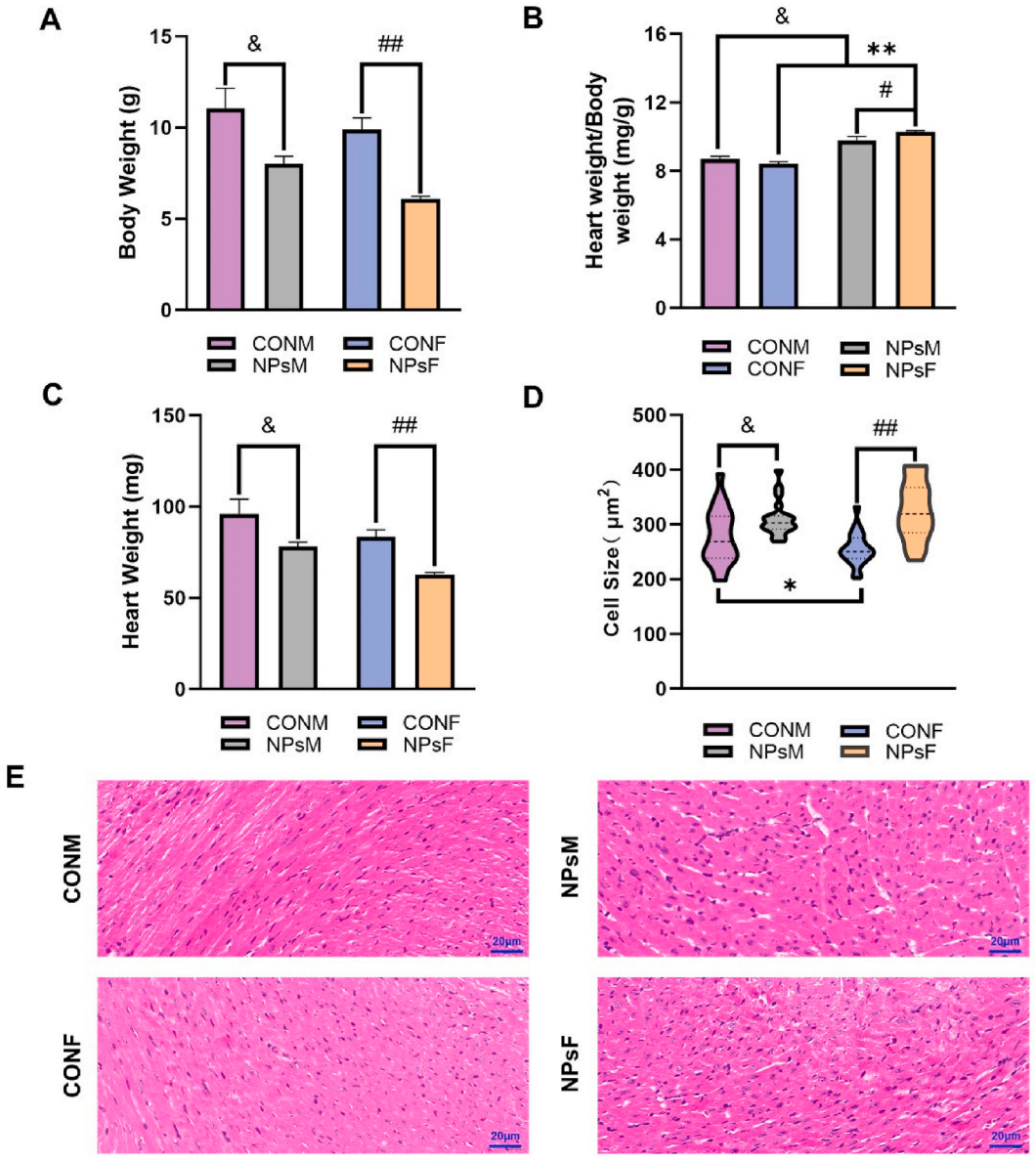

Fig. 2. The effect of maternal PS-NPs exposure on the offspring mice. (**A**) Body weights of the offspring mice obtained from control male (CONM), control female (CONF), PS-NPs-treated male (NPsM), and PS-NPs-treated female (NPsF), $^{\&}P < 0.05$, $^{\#\#}P < 0.01$. (**B**) Ratio of heart weight to body weight (HW/BW) of CONM, NPsM, CONF, and NPsF, $^{\&}P < 0.05$, $^{\#}P < 0.05$, $^{**}P < 0.01$. (**C**) Heart weights of the offspring mice obtained from CONM, CONF, NPsM, and NPsF, $^{\&}P < 0.05$, $^{\#\#}P < 0.01$. (**D**) Cell size in heart tissue of CONM, NPsM, CONF, and NPsF, $^{\&}P < 0.05$, $^{*}P < 0.05$, $^{\#\#}P < 0.01$. (**E**) Histopathology of the cardiac tissue obtained from CONM, NPsM, CONF, and NPsF, the representative micrographs of cardiac sections stained with HE staining. The scale bar represents 20 μm.

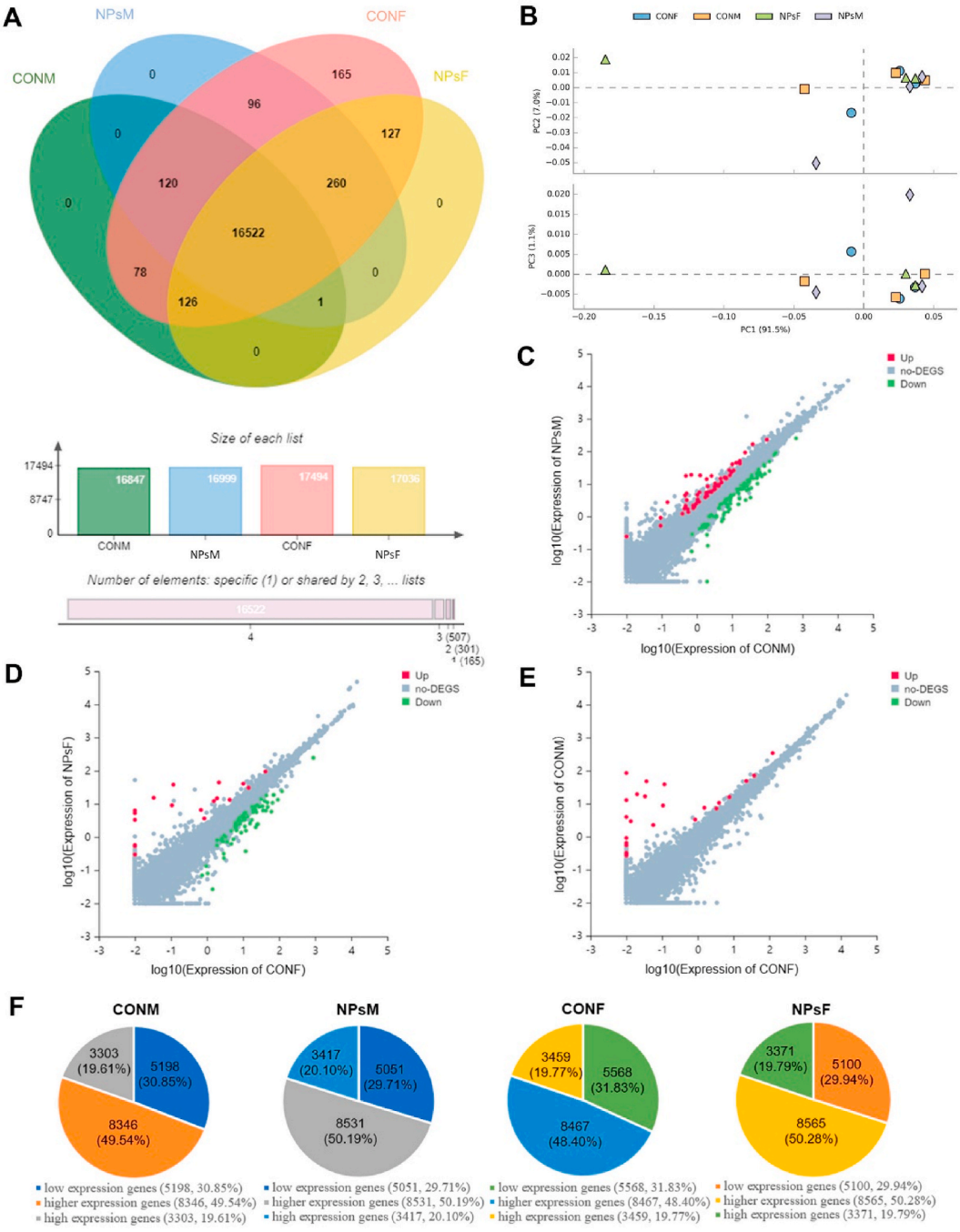

Fig. 3. PS-NPs alters transcriptome composition in the heart of offspring mice. (**A**) Venn diagram of cardiac transcriptomes of normal and PS-NPs-treated heart in male offspring mice (CONM, NPsM) and female offspring mice (CONF, NPsF); three mice in each group. (**B**) PCA scatter plot of gene expression in the heart from CONM, NPsM, CONF, and NPsF. Orange dots represent the CONM group, lavender dots represent the NPsM group, blue dots represent the CONF group, and green dots represent the NPsF group. (**C-E**) Scatter plot of DEGs was compared between the CONM and NPsM groups ***(C)***, CONF and NPsF groups ***(D)***, and CONM and CONF groups ***(E)***, respectively. The X-axis and Y-axis represents gene expression per group. Red dots represent up-regulated genes and green dots represent down-regulated genes. (**F**) Pie charts of the low, higher, and highly expressed genes in CONM, NPsM, CONF, and NPsF. Three mice in each group. (For interpretation of the references to color in this figure legend, the reader is referred to the Web version of this article.)

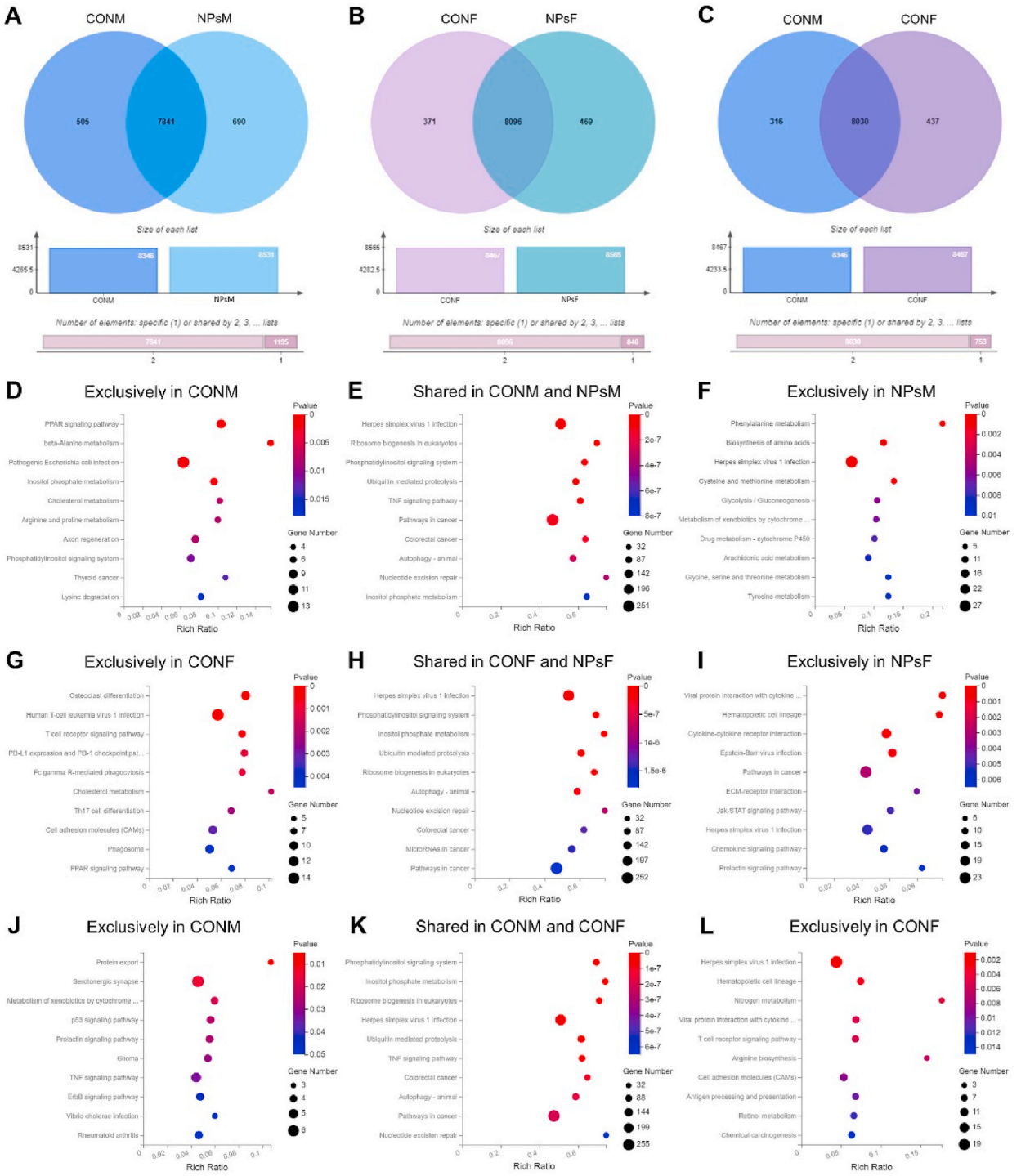

Fig. 4. PS-NPs alters KEGG pathways with sex-specific effects in the heart of offspring mice. (**A-C**) Venn diagram of higher expression genes for CONM and NPsM group ***(A)***, CONF and NPsF group ***(B)***, and CONM and CONF group ***(C)***; three mice in each group. (**D-F**) Gene annotation of top 10 KEGG pathways enriched in higher expression genes between the CONM group and NPsM group, $P < 0.05$. Among, (**D**) exclusively in CONM; (**E**) shared in CONM and NPsM; (**F**) exclusively in NPsM. (**G-I**) Gene annotation of top 10 KEGG pathways enriched in higher expression genes between the CONF group and NPsF group, $P < 0.05$. Among, (**G**) exclusively in CONF; (**H**) shared in CONF and NPsF; (**I**) exclusively in NPsF. (**J-L**) Gene annotation of top 10 KEGG pathways enriched in higher expression genes between the CONM group and CONF group, $P < 0.05$. Among, (**J**) exclusively in CONM; (**K**) shared in CONM and CONF; (**L**) exclusively in CONF.

3. Results

3.1. Maternal exposure to PS-NPs changes the size of cardiomyocytes in mouse offspring

To investigate the effects of maternal PS-NPs exposure on the birth weight and cardiomyocyte size of the offspring, including potential sex differences, we measured the body weight and heart weight of the newborn mice. A two-way between-topics ANOVA (sex with two aspects, including female and male, and PS-NPs with two aspects, including non-PS-NPs treated and PS-NPs-treated), showed that the sex × PS-NPs interaction was significant ($P < 0.05$), in addition to the significant main effects of PS-NPs ($P < 0.001$) on the body weight of offspring. Analysis of these results showed that the PS-NPs treatment had a clear effect on the body weight of the offspring, and the PS-NPs-treated group were significantly lower than the normal group (Fig. 2A). The heart weights of the offspring mice were weighed to highlight the effects of PS-NPs on the heart. Next, the heart weight/body weight (namely, HW/BW) ratio was calculated. As shown in Fig. 2B, the ANOVA performed a meaningful influence of PS-NPs ($P < 0.001$) and sex ($P = 0.04$) but not sex × PS-NPs interplay ($P = 0.078$) on HW/BW. Our analysis revealed a significant reduction in absolute heart weight in both male and female offspring of the PS-NPs-treated group compared to controls (Fig. 2C). Despite this, the HW/BW ratio was significantly elevated in the PS-NPs-treated group (Fig. 2B), driven by a greater reduction in body weight relative to heart weight in these offspring. Following this, the HE staining was demonstrated to research the influence of PS-NPs on the size of the cardiomyocytes. For cell size, the ANOVA performed a meaningful sex × PS-NPs interplay ($P = 0.027$) as well as a meaningful influence of PS-NPs ($P < 0.001$) (Fig. 2D). Cardiomyocyte size was observed to be significantly greater in male offspring of the PS-NPs-treated group than in the non-PS-NPs-treated group. However, a significant difference in cardiomyocyte size was observed between PS-NPs-treated female mice and the control group (Fig. 2D–E). In addition, the normal group of male mice exhibited slightly larger cardiomyocyte than female mice. Overall, these results indicate that maternal PS-NPs intake affects cardiac development in mouse offspring, with possible sex differences.

3.2. PS-NPs reprogram transcriptome composition of mouse offspring's heart

To investigate how maternal exposure to PS-NPs affects gene expression of the offspring's heart, we conducted transcriptome tests and performed data analysis on male and female offspring heart tissue of pregnant mice. For male mouse offspring, 16,847 and 16,999 transcripts were revealed in the non-PS-NPs-treated (CONM) heart and PS-NPs-treated (NPsM) heart, respectively. For female mouse offspring, 17,494 and 17,036 transcripts were revealed in the hearts of the non-PS-NPs-treated (CONF) heart and the PS-NPs-treated (NPsF) heart, respectively. Compared to the same-sex control group, the CONM group had 152 undetected genes, while the NPsF group had 458 undetected genes. This discrepancy is likely due to the expression levels of these genes falling below the detection threshold (Fig. 3A). Subsequently, twelve variables of transcriptome were reduced in dimensionality, and PCA was used to visualize the differences between the CONM and NPsM groups, as well as between the CONF and NPsF groups. The three principal components (PC1, PC2, and PC3) accounted for 91.50 %, 7.00 %, and 1.10 % of the total variance, respectively. This suggests that genes within the normal and PS-NPs groups displayed clustering characteristics, while there was a noticeable dispersion between these groups (Fig. 3B). The Venn and PCA results revealed a sex-specific effect of maternal PS-NPs exposure on the cardiac transcriptome of the progeny mice. As shown in Fig. 3C–E, the volcano plot of DEGs was used to illustrate the distinctions between the CONM and NPsM groups, the CONF and NPsF groups, and the CONM and CONF groups, respectively. In the scatter plot, the $Q < 0.05$ was defined as the cut-off criterion for a significantly different. Red dots indicate significant upregulation, green dots indicate significant downregulation, and gray dots indicate no significant difference. In the CONM and NPsM groups, 279 DEGs were identified, comprising 105 upregulated genes and 174 downregulated genes (Fig. 3C and Table S2). In the CONF and NPsF groups, 114 DEGs were identified, comprising 24 upregulated genes and 90 downregulated genes (Fig. 3D and Table S3). In the CONM and CONF groups, 37 DEGs were identified, comprising 30 upregulated genes and 7 downregulated genes (Fig. 3E and Table S4). Next, gene expression levels were analyzed in the CONM, NPsM, CONF, and NPsF groups to study the effect of maternal exposure to PS-NPs on the cardiac transcriptome. In accordance with previous reports [42,43], the transcripts have been divided into three types according to the groups to which they belong: low expression of genes, higher expression of genes, and highly expressed of genes. The findings are presented in Fig. 3F. For male offspring, the number of genes with low, higher, and highly expression levels were 5198 (30.85 %), 8346 (49.54 %), and 3303 (19.61 %), respectively, out of a total of 16,847 transcripts in the CONM-treated heart. From the 16,999 transcripts in the NPsM-treated heart, the low, higher, and highly expression genes accounted for 5051 (29.71 %), 8531 (50.19 %), and 3417 (20.10 %). However, in the CONF-treated hearts of female offspring, the low, higher, and highly expressed genes constituted 5568 (31.83 %), 8467 (48.40 %), and 3459 (19.77 %) of 17, 494 transcripts, respectively. In the NPsF-treated hearts, these categories accounted for 5100 (29.94 %), 8565 (50.28 %), and 3371 (19.79 %) of 17,036 transcripts, respectively. Collectively, these findings demonstrated that maternal PS-NPs exposure changed heart transcriptome composition of offspring mice with gender-specific variations.

3.3. PS-NPs affect the KEGG pathway of offspring

To examine the impact of maternal ingestion of PS-NPs on the higher expression of genes (main screening criteria: $1 \leq FPKM < 20$) and on the KEGG pathway of the genes in the offspring mice hearts, we compared the higher expression genes using Venn plots and conducted KEGG enrichment analyses (Fig. 4). Initially, transcriptome gene expression differences between the CONM and NPsM groups, as well as the CONF and NPsF groups, were compared, with the results presented in Fig. 4A–B. Male offspring, the Venn plots illustrate that out of the higher expression genes, 505 (5.59 %) genes have been exclusively to the CONM group, 7841 (86.77 %) genes

have been shared by both the CONM group and the NPsM group, and 690 (7.64 %) genes have been exclusively to the NPsM group (Fig. 4A). Similarly, Fig. 4B illustrates that in female offspring, the Venn plots illustrate that out of the higher expression genes, 371 (4.15 %) genes have been exclusively to the CONF group, 8096 (90.60 %) genes have been shared by both the CONF group and the NPsF group, and 469 (5.25 %) genes have been exclusively to the NPsF group. Additionally, we compared variations in high-expression genes in the CONM and CONF groups. This graph shows that there were 316 (3.59 %) genes that have been included solely in the CONM group, 8030 (91.43 %) genes that have been shared by both the CONM and CONF groups, and 437 (4.98 %) genes that have been included solely in the CONF group, as shown by the Venn plots (Fig. 4C).

To evaluate the impact of maternal intake of PS-NPs on KEGG pathways, KEGG enrichment analyses were conducted on the genes from the CONM, NPsM, CONF, and NPsF groups, as well as those shared between the CONM and NPsM, CONF and NPsF, and CONM and CONF groups, as illustrated in Fig. 4D–L. For male offspring, 26 KEGG functional pathways ($P < 0.05$) specific to the CONM group were discovered and classified into six distinct types: (1) environmental information processing: hippo signaling pathway-multiple species ($P = 2.61E-02$), phosphatidylinositol signaling system ($P = 1.11E-02$), hippo signaling pathway-fly ($P = 2.55E-02$), and AMPK signaling pathway ($P = 3.81E-02$); (2) genetic information processing: spliceosome ($P = 4.70E-02$); (3) cellular processes: p53 signaling pathway ($P = 3.18E-02$) and endocytosis ($P = 3.52E-02$); (4) human diseases: pathogenic *Escherichia coli* infection ($P = 1.83E-03$), thyroid cancer ($P = 1.30E-02$), insulin resistance ($P = 1.99E-02$), hepatocellular carcinoma ($P = 2.73E-02$), gastric cancer ($P = 3.29E-02$), shigellosis ($P = 3.42E-02$), and transcriptional mis-regulation in cancer ($P = 3.51E-02$); (5) metabolism: beta-Alanine metabolism ($P = 1.07E-03$), inositol phosphate metabolism ($P = 2.20E-03$), histidine metabolism ($P = 2.11E-02$), arginine and proline metabolism ($P = 7.87E-03$), lysine degradation ($P = 1.77E-02$), tryptophan metabolism ($P = 3.12E-02$), and fatty acid degradation ($P = 3.55E-02$); (6) organismal systems: cholesterol metabolism ($P = 7.23E-03$), axon regeneration ($P = 7.98E-03$), Fc gamma R-mediated phagocytosis ($P = 2.47E-02$), PPAR signaling pathway ($P = 3.02E-04$), and thyroid hormone signaling pathway ($P = 2.69E-02$) (Fig. 4D). 36 KEGG functional pathways ($P < 0.0001$) specific to shared CONM and NPsM groups were found and classified into five distinct types: (1) cellular processes: lysosome ($P = 1.37E-05$), apoptosis ($P = 1.68E-05$), autophagy-animal ($P = 2.46E-07$), and cell cycle ($P = 4.26E-05$); (2) environmental information processing: MAPK signaling pathway ($P = 1.25E-05$), notch signaling pathway ($P = 4.26E-06$), phosphatidylinositol signaling system ($P = 3.20E-08$), ErbB signaling pathway ($P = 3.20E-06$), TNF signaling pathway ($P = 4.41E-08$) and Wnt signaling pathway ($P = 8.27E-06$); (3) genetic information processing: base excision repair ($P = 9.05E-06$), DNA replication ($P = 4.33E-06$), ribosome biogenesis in eukaryotes ($P = 1.10E-09$), non-homologous end-joining ($P = 4.07E-05$), ubiquitin mediated proteolysis ($P = 3.83E-08$), nucleotide excision repair ($P = 3.08E-07$), basal transcription factors ($P = 7.39E-07$), aminoacyl-tRNA biosynthesis ($P = 3.36E-06$), RNA transport ($P = 1.91E-05$), RNA degradation ($P = 6.31E-05$), and mismatch repair ($P = 1.40E-05$); (4) human diseases: herpes simplex virus 1 infection ($P = 5.47E-11$), pathways in cancer ($P = 1.04E-07$), colorectal cancer ($P = 1.10E-07$), microRNAs in cancer ($P = 1.21E-06$), yersinia infection ($P = 4.08E-06$), pancreatic cancer ($P = 1.09E-05$), small cell lung cancer ($P = 1.80E-05$), hepatitis B ($P = 4.47E-05$), endometrial cancer ($P = 4.55E-05$), endocrine resistance ($P = 6.52E-05$), and human papillomavirus infection ($P = 3.36E-05$); (5) metabolism: inositol phosphate metabolism ($P = 7.01E-07$), N-Glycan biosynthesis ($P = 1.48E-05$), terpenoid backbone biosynthesis ($P = 4.25E-05$), and amino sugar and nucleotide sugar metabolism ($P = 9.10E-05$) (Fig. 4E). While 10 significantly KEGG pathways ($P < 0.01$) specific to the NPsM group were found and divided into two types: (1) human diseases: herpes simplex virus 1 infection ($P = 9.98E-04$); (2) metabolism: phenylalanine metabolism ($P = 7.77E-04$), cysteine and methionine metabolism ($P = 1.47E-03$), biosynthesis of amino acids ($P = 9.16E-04$), metabolism of xenobiotics by cytochrome P450 ($P = 6.30E-03$), drug metabolism-cytochrome P450 ($P = 7.40E-03$), glycolysis/gluconeogenesis ($P = 5.80E-03$), arachidonic acid metabolism ($P = 8.30E-03$), glycine, serine and threonine metabolism ($P = 9.62E-03$), and tyrosine metabolism ($P = 9.62E-03$) (Fig. 4F).

For female offspring, 17 functional pathways specific to the CONF group were significantly enriched ($P < 0.01$) and were classified into four distinct types: (1) cellular processes: phagosome ($P = 4.40E-03$) and cellular senescence ($P = 5.27E-03$); (2) environmental information processing: cell adhesion molecules (CAMs) ($P = 3.12E-03$) and viral protein interaction with cytokine and cytokine receptor ($P = 9.51E-03$); (3) human diseases: human T-cell leukemia virus 1 infection ($P = 1.07E-04$), viral carcinogenesis ($P = 7.61E-03$), acute myeloid leukemia ($P = 7.96E-03$), PD-L1 expression and PD-1 checkpoint pathway in cancer ($P = 9.23E-04$), and human immunodeficiency virus 1 infection ($P = 9.31E-03$); (4) organismal systems: osteoclast differentiation ($P = 6.77E-05$), T cell receptor signaling pathway ($P = 4.74E-04$), cholesterol metabolism ($P = 1.69E-03$), Fc gamma R-mediated phagocytosis ($P = 1.06E-03$), Th17 cell differentiation ($P = 2.20E-03$), PPAR signaling pathway ($P = 4.42E-03$), hematopoietic cell lineage ($P = 6.45E-03$), and natural killer cell mediated cytotoxicity ($P = 9.08E-03$) (Fig. 4G). 33 functional pathways specific to shared CONF and NPsF groups were significantly enriched ($P < 0.0001$) and were classified into six distinct types: (1) cellular processes: autophagy -animal ($P = 2.13E-07$); (2) genetic information processing: ubiquitin mediated proteolysis ($P = 1.24E-08$), ribosome biogenesis in eukaryotes ($P = 1.79E-08$), nucleotide excision repair ($P = 7.57E-07$), DNA replication ($P = 1.71E-06$), basal transcription factors ($P = 1.78E-06$), aminoacyl-tRNA biosynthesis ($P = 7.68E-06$), base excision repair ($P = 1.82E-05$), mismatch repair ($P = 2.42E-05$), RNA transport ($P = 4.28E-05$), non-homologous end-joining ($P = 6.04E-05$), and RNA degradation ($P = 6.89E-05$); (3) environmental information processing: phosphatidyl inositol signaling system ($P = 8.86E-11$), notch signaling pathway ($P = 2.94E-06$), TNF signaling pathway ($P = 3.56E-06$), Wnt signaling pathway ($P = 9.20E-06$), hippo signaling pathway-fly ($P = 2.00E-05$), ErbB signaling pathway ($P = 2.63E-05$), and MAPK signaling pathway ($P = 5.46E-05$); (4) human diseases: small cell lung cancer ($P = 2.22E-05$), herpes simplex virus 1 infection ($P = 7.51E-13$), colorectal cancer ($P = 1.24E-06$), microRNAs in cancer ($P = 1.37E-06$), pancreatic cancer ($P = 7.87E-05$), pathways in cancer ($P = 1.70E-06$), yersinia infection ($P = 6.90E-06$), and non-small cell lung cancer ($P = 9.46E-05$); (5) metabolism: N-Glycan biosynthesis ($P = 9.62E-06$), inositol phosphate metabolism ($P = 1.67E-10$), pyrimidine metabolism ($P = 1.12E-05$), seleno-compound metabolism ($P = 2.10E-05$), and amino sugar and nucleotide sugar metabolism ($P = 6.07E-05$); (6) organismal systems: thyroid hormone signaling pathway ($P = 1.76E-05$) (Fig. 4H). While 11 functional pathways specific to the NPsF group were significantly

enriched (P < 0.01) and were classified into four distinct types: (1) human diseases: Epstein-Barr virus infection (P = 6.88E-04), pathways in cancer (P = 2.80E-03), and herpes simplex virus 1 infection (P = 4.82E-03); (2) cellular processes: cellular senescence (P = 9.44E-03); (3) organismal systems: hematopoietic cell lineage (P = 2.92E-04), chemokine signaling pathway (P = 5.64E-03), and prolactin signaling pathway (P = 6.03E-03); (4) environmental information processing: viral protein interaction with cytokine and cytokine receptor (P = 1.10E-04), cytokine-cytokine receptor interaction (P = 4.31E-04), ECM-receptor interaction (P = 3.99E-03), and Jak-STAT signaling pathway (P = 4.64E-03) (Fig. 4I). These results indicate that the offspring's heart express different transcripts.

Therefore, we also in comparison to the genes of the CONM and the CONF groups using KEGG enrichment analysis. A total of 12

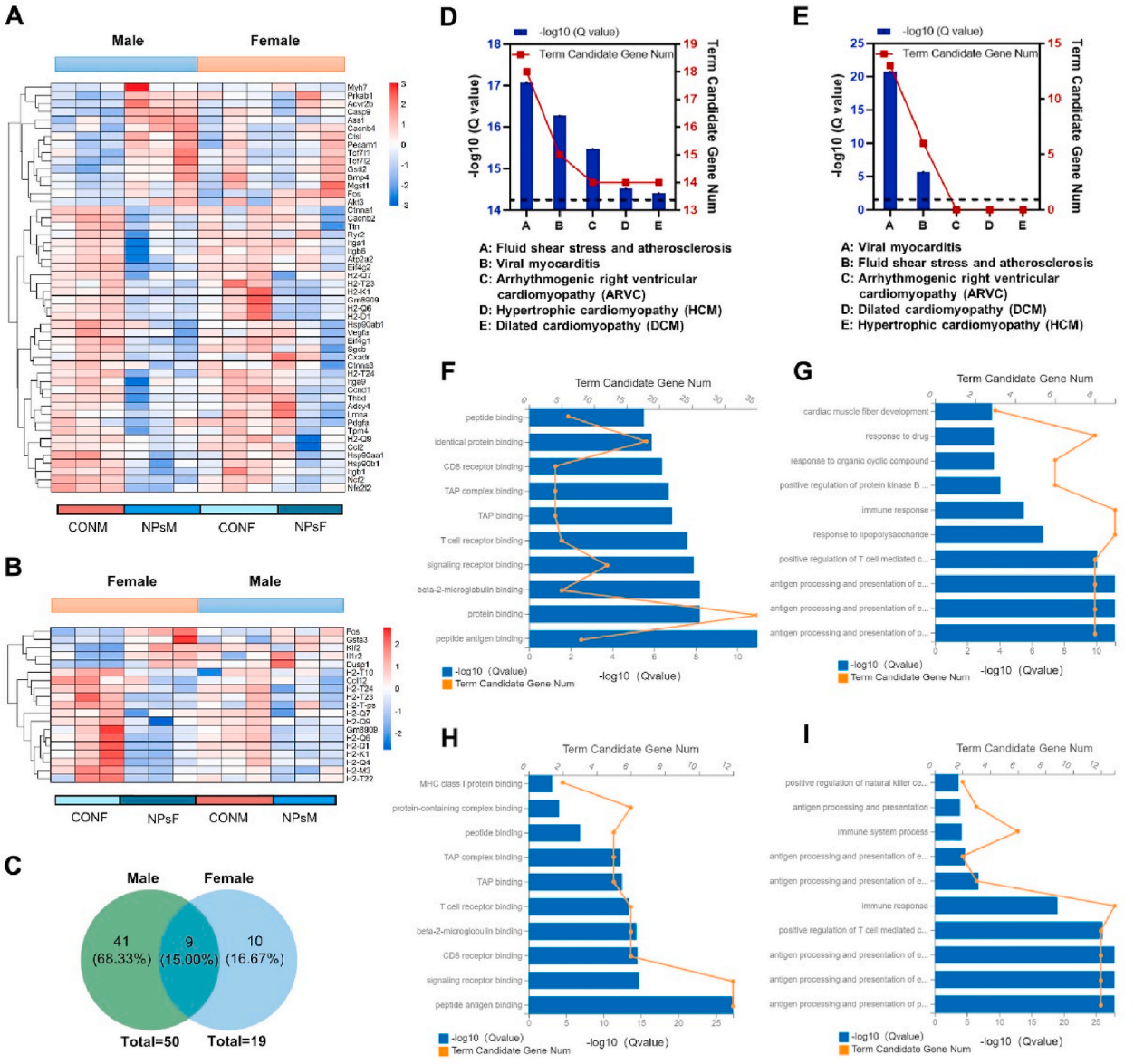

Fig. 5. PS-NPs alters the expression profile of genes associated with cardiovascular disease and causes different cardiac disease of the offspring mice. (**A**–**B**) Heatmaps of the cardiovascular disease-associated DEGs in heart tissue of the male ***(A)*** and female ***(B)*** offspring mice. The color bar indicates the scale used to show the expression of genes with the expression range normalized to ±2. (**C**) Venn diagram of DEGs associated with cardiovascular disease for the NPsM group and NPsF group. (**D-E**) Gene annotation of KEGG pathways enriched in cardiovascular disease-associated genes in heart tissue of the NPsM group ***(D)*** and the NPsF group ***(E)***, with $P < 0.05$. The top 10 pathways are shown. (**F-G**) Gene annotation of molecular function ***(F)*** and biological process ***(G)*** of GO enriched in cardiovascular disease-associated genes for heart tissue of male offspring mice, with $P < 0.05$ (N = 3 individual mice per group). The top 10 terms are shown. (**H-I**) Gene annotation of molecular function ***(H)*** and biological process ***(I)*** of GO enriched in cardiovascular disease-associated genes for heart tissue of female offspring mice, with $P < 0.05$ (N = 3 individual mice per group). The top 10 terms are shown. (For interpretation of the references to color in this figure legend, the reader is referred to the Web version of this article.)

KEGG pathways ($P < 0.05$) specific to the CONM group were found and divided into six types: (1) environmental information processing: TNF signaling pathway ($P = 3.20E-02$), ErbB signaling pathway ($P = 4.24E-02$), and cell adhesion molecules (CAMs) ($P = 4.93E-02$); (2) cellular processes: p53 signaling pathway ($P = 2.49E-02$); (3) genetic information processing: protein export ($P = 9.24E-03$); (4) human diseases: glioma ($P = 2.85E-02$), vibrio cholerae infection ($P = 4.31E-02$), and rheumatoid arthritis ($P = 4.56E-02$); (5) metabolism: metabolism of xenobiotics by cytochrome P450 ($P = 2.06E-02$) and terpenoid backbone biosynthesis ($P = 4.97E-02$); (6) organismal systems: serotonergic synapse ($P = 1.67E-02$) and prolactin signaling pathway ($P = 2.60E-02$) (Fig. 4J). A total of 7 functional pathways specific to the CONF group were significantly enriched ($P < 0.01$) and were classified into four distinct types: (1) environmental information processing: cell adhesion molecules (CAMs) ($P = 9.37E-03$) and viral protein interaction with cytokine and cytokine receptor ($P = 5.65E-03$); (2) human diseases: herpes simplex virus 1 infection ($P = 1.84E-03$); (3) metabolism: nitrogen metabolism ($P = 5.03E-03$) and arginine biosynthesis ($P = 6.96E-03$); (4) organismal systems: hematopoietic cell lineage ($P = 3.60E-03$) and T cell receptor signaling pathway ($P = 5.96E-03$) (Fig. 4L). Totals of 132 functional pathways of shared in CONF and CONM were significantly enriched ($P < 0.05$), of which 9 pathways were the same as the pathways unique to CONF and CONM, which are TNF signaling pathway ($P = 4.97E-08$), ErbB signaling pathway ($P = 1.99E-05$), p53 signaling pathway ($P = 1.19E-02$), glioma ($P = 2.54E-02$), herpes simplex virus 1 infection ($P = 8.14E-10$), PD-L1 expression and PD-1 checkpoint pathway in cancer ($P = 3.92E-02$), terpenoid backbone biosynthesis ($P = 3.40E-04$), pyrimidine metabolism ($P = 8.46E-05$), and osteoclast differentiation ($P = 5.62E-03$) (Fig. 4K). In summary, these results demonstrate that maternal intake of PS-NPs induces sex-specific alterations in the KEGG pathways of the mouse heart.

3.4. PS-NPs induce sex-specific cardiovascular disease in offspring mice

According to evidence from clinical trials, maternal exposure to pollutants is linked to cardiovascular and circulatory diseases in offspring. To assess the impact of maternal intake of PS-NPs, we initially contrasted the cardiovascular disease-related transcript expression in male and female offspring mice hearts between those fed normal water and those fed water with PS-NPs during experimental session. As shown in the Venn diagram, in the PS-NPs-treated group, 41 genes (68.33 %) were unique to the male offspring, 10 genes (16.67 %) were unique to the female offspring, and 9 genes (15.00 %) were common to the male and female offspring (Fig. 5C). In addition, the heatmap reveals higher expression of genes linked to cardiovascular disease in PS-NPs offspring mice compared to controls, with greater prominence in male offspring mice (Fig. 5A–B).

Further, we found obvious distinction in the notable KEGG pathway in the hearts of the offspring mice, after analyzing the KEGG pathway of genes associated with cardiovascular disease. For male offspring mice, the KEGG enrichment analysis revealed that the pathways related to cardiovascular disorders mainly consist of fluid shear stress and atherosclerosis ($P = 4.55E-20$), viral myocarditis ($P = 5.73E-19$), arrhythmogenic right ventricular cardiomyopathy (ARVC) ($P = 5.33E-18$), hypertrophic cardiomyopathy (HCM) ($P = 6.41E-17$), and dilated cardiomyopathy (DCM) ($P = 1.03E-16$) (Fig. 5D). Next, we carried out the enrichment analysis of transcripts in GO molecular function and biological processes that were associated with cardiovascular disease in male offspring. As shown by the results in Fig. 5F, the molecular function can be classed into one category ($P < 0.05$, the top 10 pathways are shown): binding: peptide antigen binding ($P = 5.41E-14$); protein binding ($P = 7.30E-11$); beta-2-microglobulin binding ($P = 9.32E-11$); signaling receptor binding ($P = 2.43E-10$); T cell receptor binding ($P = 6.15E-10$); TAP binding ($P = 4.05E-09$); TAP complex binding ($P = 6.74E-09$); CD8 receptor binding ($P = 1.58E-08$); identical protein binding ($P = 5.82E-08$); peptide binding ($P = 1.53E-07$). As illustrated in Fig. 5G, biological process in the male offspring can be classed into five types ($P < 0.05$, the top 10 pathways are shown): (1) biological regulation: positive regulation of T cell mediated cytotoxicity ($P = 3.37E-13$) and positive regulation of protein kinase B signaling ($P = 5.99E-07$); (2) cellular process: cardiac muscle fiber development ($P = 2.93E-06$); (3) immune system process: antigen processing and presentation of endogenous peptide antigen via MHC class I via ER pathway, antigen processing and presentation of peptide antigen via MHC class I ($P = 1.17E-14$), antigen processing and presentation of endogenous peptide antigen via MHC class Ib ($P = 1.95E-14$), TAP-independent ($P = 1.95E-14$), and immune response ($P = 1.81E-08$); (4) multi-organism process: response to lipopolysaccharide ($P = 9.66E-10$); (5) response to stimulus: response to drug ($P = 2.00E-06$) and response to organic cyclic compound ($P = 1.73E-06$).

For female offspring mice, the KEGG enrichment analysis revealed that the pathways related to cardiovascular disease mainly included viral myocarditis ($P = 1.19E-22$) and fluid shear stress and atherosclerosis ($P = 4.65E-07$) (Fig. 5E). Meanwhile, GO enrichment analysis also showed a difference. As illustrated in Fig. 5H, the molecular function in the female offspring can be classed into one category ($P < 0.05$, the top 10 pathways are shown): binding: peptide antigen binding ($P = 1.00E-29$), signaling receptor binding ($P = 6.66E-17$), CD8 receptor binding ($P = 1.75E-16$), beta-2-microglobulin binding ($P = 3.25E-16$), T cell receptor binding ($P = 3.51E-15$), TAP binding ($P = 3.74E-14$), TAP complex binding ($P = 7.47E-14$), peptide binding ($P = 2.02E-08$), protein-containing complex binding ($P = 1.53E-05$), and MHC class I protein binding ($P = 1.40E-04$). In addition, as can be seen in Fig. 5I, the biological process were classed into two types ($P < 0.05$, the top 10 pathways are shown): (1) immune system process: antigen processing and presentation of peptide antigen via MHC class I ($P = 8.51E-31$), antigen processing and presentation of endogenous peptide antigen via MHC class Ib ($P = 1.94E-30$), antigen processing and presentation of endogenous peptide antigen via MHC class I via ER pathway, TAP-independent ($P = 1.94E-30$), positive regulation of T cell mediated cytotoxicity ($P = 1.88E-28$), immune response ($P = 2.54E-21$), antigen processing and presentation of endogenous peptide antigen via MHC class I via ER pathway, TAP-dependent ($P = 5.63E-09$), antigen processing and presentation of exogenous peptide antigen via MHC class Ib ($P = 7.24E-07$), immune system process ($P = 2.74E-06$), and antigen processing and presentation ($P = 5.88E-06$); (2) multicellular organismal process: positive regulation of natural killer cell cytokine production ($P = 1.08E-05$). Taken together, the analysis of KEGG pathway and GO enrichment results indicate that maternal intake of PS-NPs may be linked to an elevated risk of cardiovascular disease and related conditions in offspring.

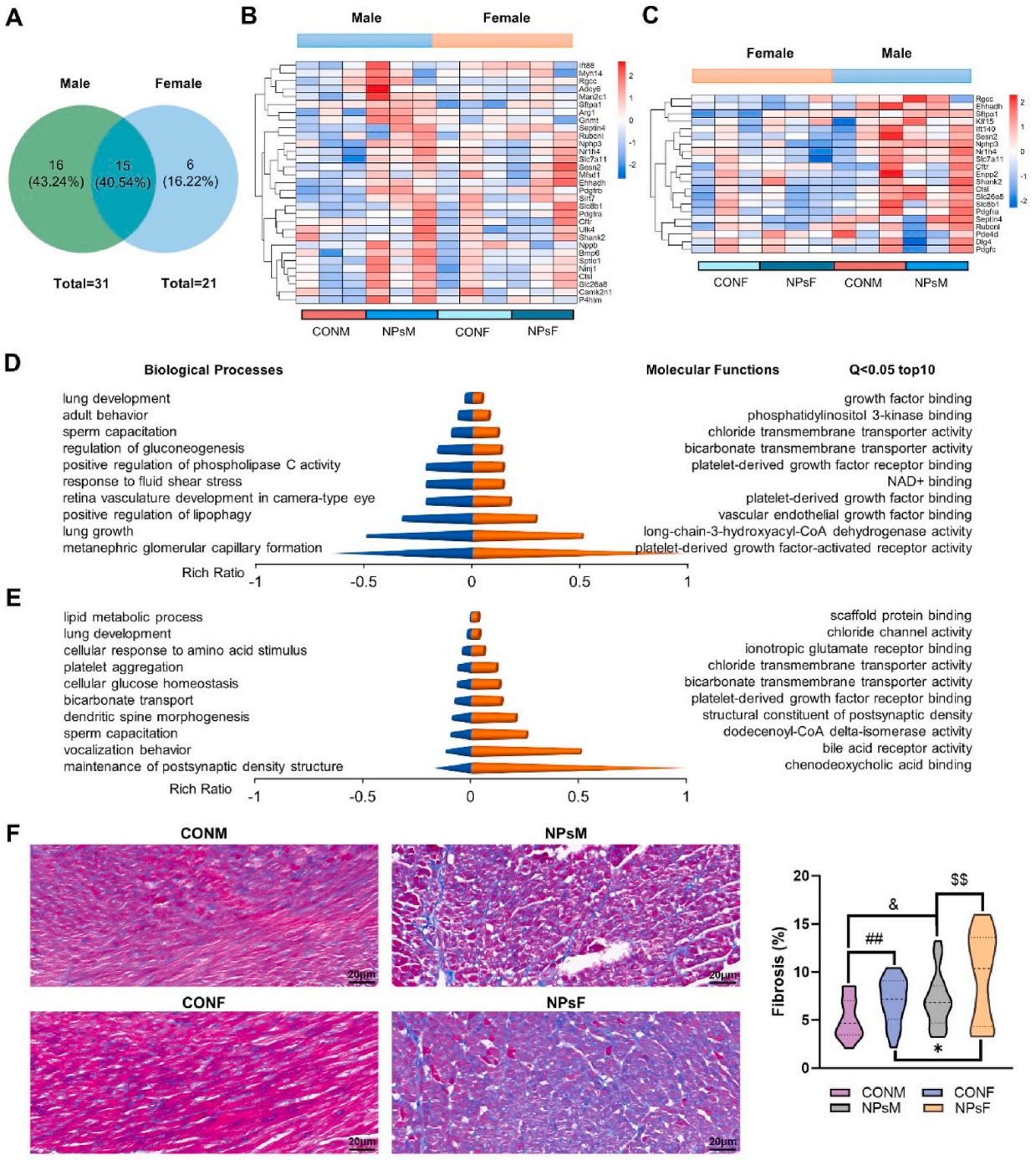

Fig. 6. PS-NPs alters the expression profile of genes associated with fibrosis in the heart of offspring. (**A**) Venn diagram of DEGs associated with fibrosis for PS-NPs-treated heart tissue of the offspring mice. (**B**–**C**) Heatmaps of the fibrosis-associated genes in heart tissue of the NPsM group ***(B)*** and the NPsF group ***(C)***. The color bar indicates the scale used to show the expression of genes with the expression range normalized to ±2. (**D**–**E**) Gene annotation of molecular function and biological process of GO enriched terms for fibrosis-associated genes for heart tissue of mice, with $Q < 0.05$, the top 10 terms were shown. Among, the male offspring mice ***(D)*** and the female offspring mice ***(E)***, three mice in each group. (**F**) Representative immunohistochemical images with CONM, NPsM, CONF, and NPsF. The scale bar represents 20 μm. Quantification of fibrosis measured as a percentage of total myocardial area in heart of the control group compared with the PS-NPs-treated group. $^{\&}P < 0.05$, $^{*}P < 0.05$, $^{\#\#}P < 0.01$, $^{\$\$}P < 0.01$. (For interpretation of the references to color in this figure legend, the reader is referred to the Web version of this article.)

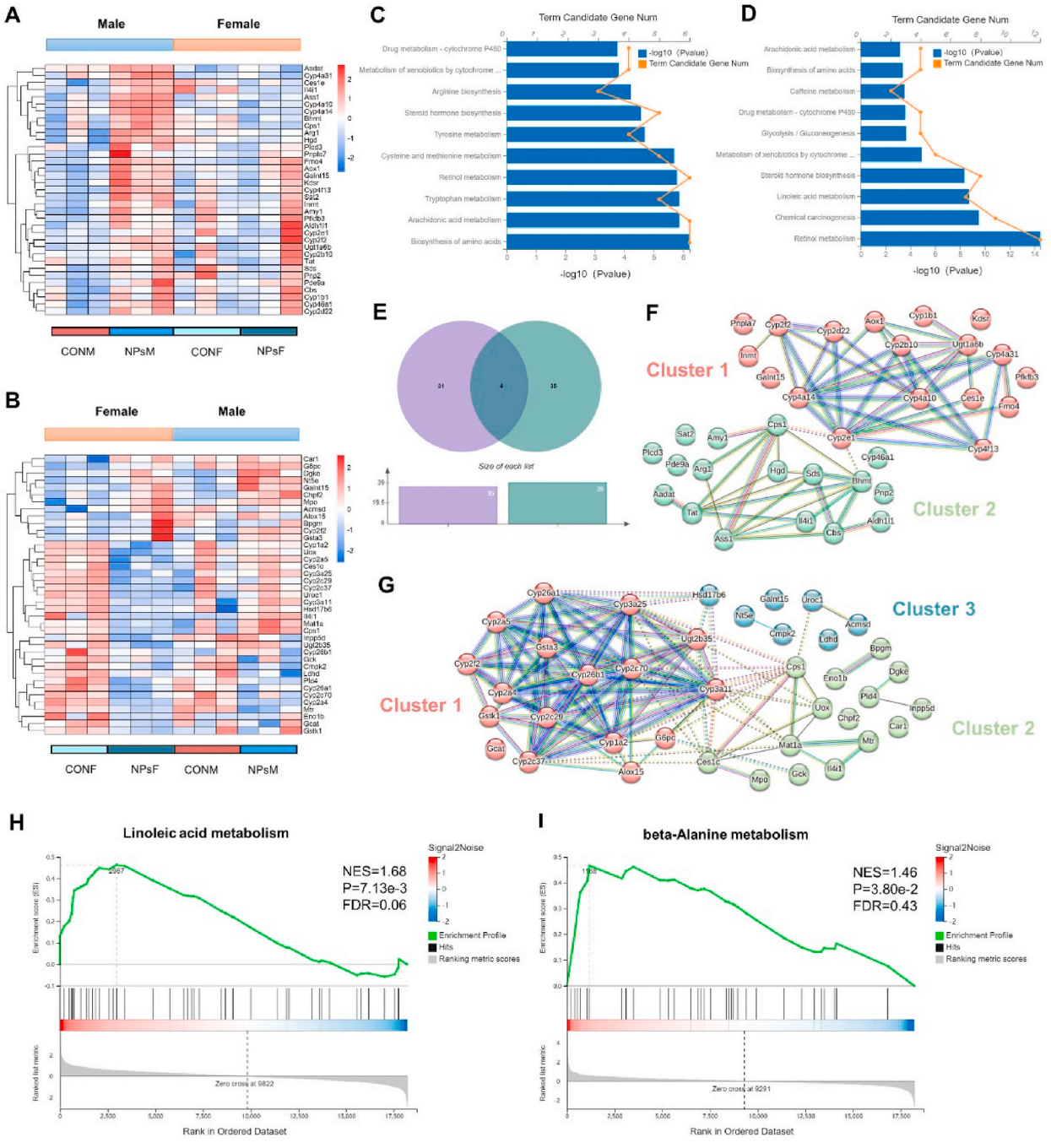

Fig. 7. PS-NPs alters the expression profile of genes related to metabolism in the heart of offspring. (**A-B**) Heatmaps of the genes related to metabolism in heart tissue of the NPsM group ***(A)*** and the NPsF group ***(B)***. The color bar indicates the scale used to show the expression of genes with the expression range normalized to ±2. (**C-D**) Gene annotation of KEGG pathways enriched in metabolism-associated genes in heart tissue of the NPsM group ***(C)*** and the NPsF group ***(D)***, with $P < 0.05$. The top 10 pathways are shown. (**E**) Venn diagram of DEGs related to metabolism of the NPsM group and the NPsF group. (**F-G**) The PPANs of the metabolism-associated genes in heart of male offspring mice ***(F)*** and female offspring mice ***(G)***, three mice in each group. (**H-I**) The GSEA analysis of the metabolism-associated genes in heart of male offspring mice ***(H)*** and female offspring mice ***(I)***, three mice in each group. (For interpretation of the references to color in this figure legend, the reader is referred to the Web version of this article.)

3.5. PS-NPs increase fibrosis of mouse offspring's heart

In normotensive rats, exposure to PS-NPs has been strongly associated with the onset and progression of cardiac fibrosis. Therefore, by assessing the differential analysis in the levels of transcripts associated with fibrosis, we investigated the effect of the maternal intake of PS-NPs on the distinct molecular and biological characteristics associated with fibrosis in the hearts of mouse offspring. In male offspring, the expression of 31 fibrotic-associated transcripts differed significantly, whereas only 21 transcripts were linked to a noticeable fibrotic difference in female offspring (Fig. 6A). And, as can be seen from the results in Fig. 6B–C, regardless of gender, the expression level of genes associated with fibrosis was higher in the offspring of the PS-NPs-treated group than in the normal group, and there were different degrees of fibrosis enhancement. To confirm the RNA-seq results, we then performed qPCR to validate *Slc7a11*, *Nr1h4*, *Nppb*, *Rgcc*, *Klf15*, and *Ctsl* genes, which are involved in fibrosis. The results showed that expression of all the six genes was upregulated in the heart of offspring after PS-NPs treatment, which is consistent with RNA-seq data (Figs. S1A–F). Subsequently, the enrichment analysis in GO molecular functions and biological processes was conducted to investigate the molecular and biological characteristics of genes involved in fibrosis. According to the analysis results of this study, PS-NPs treatment can affect the molecular function and biological process of these genes in both male (Fig. 6D and Tables S5–6) and female (Fig. 6E and Table S7) offspring mice, but to different degrees. Subsequently, immunohistochemistry was employed to assess fibrosis in the hearts to determine whether maternal intake of PS-NPs accelerated its development in the offspring. The ANOVA analysis performed a meaningful main influence of sex ($F = 9.846$; $P = 0.003$) as well as a meaningful main influence of PS-NPs ($F = 11.537$; $P = 0.001$), but not sex × PS-NPs interplay ($F = 0.951$; $P = 0.343$). Masson's staining revealed that the degree of fibrosis in both male and female offspring treated with PS-NPs was significantly increased compared to the control group ($P < 0.05$) (Fig. 6F). Specifically, in the PS-NPs-treated group, the degree of cardiac fibrosis in female offspring was approximately twice that observed in male offspring (2.94 % vs. 1.65 %) (Fig. 6F–G). Taken together, the heatmap analysis, GO enrichment analysis, and Masson's staining results suggest that maternal intake of PS-NPs significantly induces cardiac fibrosis in offspring mice.

3.6. PS-NPs cause metabolic disturbance of mouse offspring's heart

Maternal factors may influence metabolic disorders in offspring. To assess the impact of maternal PS-NPs intake on metabolic processes in offspring, we compared the expression levels of metabolic-related gene transcripts between the normal group and the PS-NPs group. Results are presented in Fig. 7A. It has been discovered that PS-NPs have a detrimental effect on the expression of 35 transcript profiles of metabolism in male offspring mice, leading to a severe disorder ($P < 0.05$). Similarly, PS-NPs was also found to affect the expression of 39 transcript profiles of metabolism in female offspring, which causes a serious mess with the metabolism (Fig. 7B). To confirm the RNA-seq results, we then performed qPCR to validate *Cyp2d22, Plcd3, Inmt*, *Galnt15*, *Nt5e*, and *Dgke* genes, which are involved in metabolism. The results showed that expression of all the six genes was upregulated in the heart of offspring after PS-NPs treatment, which is consistent with RNA-seq data (Figs. S2A–F).

To investigate whether the effects of PS-NPs on metabolism pathways were sex-different in female and male offspring, we conducted a KEGG pathway enrichment analysis (Fig. 7C–D) of metabolism-related genes and showed the distribution of these transcripts by Venn diagrams (Fig. 7E). For the male offspring, a total of 13 pathways ($P < 0.001$) have been identified, which can be divided into 5 types, namely: (1) amino acid metabolism: tryptophan metabolism ($P = 1.33E-06$), cysteine and methionine metabolism ($P = 2.00E-06$), tyrosine metabolism ($P = 1.99E-05$), arginine biosynthesis ($P = 5.94E-05$), phenylalanine, tyrosine and tryptophan biosynthesis ($P = 4.55E-04$), alanine, aspartate and glutamate metabolism ($P = 4.90E-04$), and glycine, serine and threonine metabolism ($P = 5.71E-04$); (2) global and overview maps: biosynthesis of amino acids ($P = 6.01E-07$); (3) lipid metabolism: arachidonic acid metabolism ($P = 1.33E-06$), and steroid hormone biosynthesis ($P = 2.71E-05$); (4) metabolism of cofactors and vitamins: retinol metabolism ($P = 1.62E-06$); (5) xenobiotics biodegradation and metabolism: metabolism of xenobiotics by cytochrome P450 ($P = 1.54E-04$), and drug metabolism-cytochrome P450 ($P = 1.73E-04$) (Fig. 7C). For the female offspring, a total of 10 pathways ($P < 0.001$) have been identified, which can be divided into 6 types, namely: (1) biosynthesis of other secondary metabolites: caffeine metabolism ($P = 3.05E-04$); (2) carbohydrate metabolism: glycolysis/gluconeogenesis ($P = 2.23E-04$); (3) global and overview maps: biosynthesis of amino acids ($P = 4.04E-04$); (4) lipid metabolism: linoleic acid metabolism ($P = 1.83E-09$), steroid hormone biosynthesis ($P = 4.56E-09$), and arachidonic acid metabolism ($P = 6.72E-04$); (5) metabolism of cofactors and vitamins: retinol metabolism ($P = 3.36E-15$); (6) xenobiotics biodegradation and metabolism: metabolism of xenobiotics by cytochrome P450 ($P = 1.23E-05$), drug metabolism-cytochrome P450 ($P = 2.65E-04$), and drug metabolism-other enzymes ($P = 6.72E-04$) (Fig. 7D). Venn diagrams show that in the male offspring mice treated with PS-NPs, 31 genes (44.28 %) were unique, whereas in the female offspring mice treated with HSD, 35 genes (50.00 %) were unique (Fig. 7E). Next, this study further investigates the correlation and function of genes associated metabolism by transcripts' PPAN. The main findings, presented in Fig. 7F–G, reveal a complex interaction of metabolism-associated genes corresponding to KEGG pathways in offspring. In addition, GSEA analysis revealed a significant enrichment of metabolic dysfunction in male offspring mice, while no such enrichment was observed in female offspring mice. For male offspring mice, twelve metabolic pathways were significantly enriched; like one of them, linoleic acid metabolism, NES = 1.68, $P = 7.13e-3$, FDR = 0.06 (Fig. 7H). However, only one metabolic pathway showed enrichment in male offspring mice that did not meet the criteria: beta-Alanine metabolism, NES = 1.46, $P = 3.80e-2$, FDR = 0.43 (the value of FDR was not less than 0.25) (Fig. 7I). In summary, the results of these studies show that maternal intake of PS-NPs alters the metabolic expression profile and accelerates metabolic disruption in the hearts of offspring mice.

3.7. PS-NPs cause immunologic derangement of mouse offspring's heart

Exposure to PS-NPs has been reported to be associated with immune cell infiltration leading to adverse cardiac effects. CD68 is primarily used to label macrophages in tissue cells. Hence, we carried out IHC to identify the CD68, a marker of macrophage, and determine whether macrophage infiltration in the heart tissue increases with maternal intake of PS-NPs. The accuracy of the experimental results was confirmed by the $CD68^{+}$ cells. An ANOVA analysis performed no meaningful sex × PS-NPs interplay ($P = 0.198$), and maternal exposure to PS-NPs enhances macrophage infiltration in the heart tissue of the offspring (Fig. 8A). To confirm the effect of maternal intake of PS-NPs on the immune-related molecular characteristics of the heart of the offspring, we analyzed the variation in the levels of immune-related transcripts. Heatmap revealed that maternal contact with PS-NPs has altered the expression of immune-related genes in 30 male offspring and 20 female offspring, respectively (Fig. 8B–C). To confirm the RNA-seq results, we then performed qPCR to validate *Fos*, *Rnasel*, *Plk3*, *Lcn2*, *Cd247*, and *S100a9* genes, which are involved in immunity. The results showed that expression of all the six genes was upregulated in the heart of offspring after PS-NPs treatment, which is consistent with RNA-seq data (Figs. S3A–F). In addition, Venn diagrams were also used to compare the distribution of these transcripts associated with immunity in the offspring. The results show that 22 genes (53.66 %) have been unique to the male offspring, 11 genes (26.83 %) have been unique to the female offspring, and 8 genes (19.51 %) have been shared by both females and males of offspring (Fig. 8D). Next, the immune-related genes of male and female offspring mice were analyzed for KEGG pathways and found to be significantly different. A total of 30 pathways ($P < 0.05$) have been identified in the male offspring, which can be divided into 5 types, and Fig. 8E shows the top 10 pathways. While, a total of 22 pathways ($P < 0.05$) have been identified in the female offspring, which can be divided into 4 types, and the top 10 pathways are shown in Fig. 8F. In addition, the STRING database have been utilized to graphically represent these transcripts' PPAN, with the aim of investigating the correlation and function of genes associated with immunity. As illustrated in Fig. 8G, in the male offspring, the PPANs have been divided into two distinct clusters based on their various biological procedures. These results suggest that transcripts associated with immunity in male offspring mice exhibit a certain level of complexity, with various functional pathways represented by different clusters. In contrast, only one cluster was identified in the transcripts of female offspring ($P < 0.05$) (Fig. 8H). Collectively, these results demonstrate that maternal exposure to PS-NPs alters the immune expression profile and immunological activity in the hearts of offspring mice.

3.8. PS-NPs promote apoptosis in mouse offspring's heart

Apoptosis of cardiomyocytes in offspring mice has been reported to be induced by a prenatal high-salt diet. In this study, we aimed to determine whether maternal intake of PS-NPs induces sex-specific apoptotic effects in the heart tissue of offspring by analyzing transcripts of genes related to apoptosis that exhibited significant differences. As illustrated in the heatmap, heart tissue from male and female offspring mice exposed to PS-NPs during pregnancy exhibited significant differences in transcript levels related to apoptosis compared to offspring from pregnant mice on a normal diet. In male offspring, exposure to PS-NPs resulted in 26 differentially expressed genes associated with cardiac apoptosis compared to offspring from mice on a normal diet (Fig. 9A). Similarly, 25 such genes were identified in female offspring (Fig. 9B). To confirm the RNA-seq results, we then performed qPCR to validate *Zfp36*, *Tfdp2*, *Map3k6*, *Igfbp3*, *Mkrn1*, *and Sik1* genes, which are involved in apoptosis. The results showed that expression of all the six genes was upregulated in the heart of offspring after PS-NPs treatment, which is consistent with RNA-seq data (Figs. S4A–F). Furthermore, to investigate the degree of enrichment of apoptosis-associated differential genes in GO term, we carried out the GO enrichment analysis. The results showed that the functions in molecular and biological processes of genes related to apoptosis were altered in the offspring following maternal intake of PS-NPs (Fig. 9E–F and Tables S8–11). Finally, we employed immunofluorescent staining to evaluate whether maternal PS-NPs lead to apoptosis in the hearts of offspring mice. Cleaved caspase-3, a well-known marker of apoptosis, is illustrated in Fig. 9C. Maternal PS-NPs triggered apoptosis in both male and female offspring mice when compared with the normal group. Simultaneously, the cleaved caspase-3 expression levels increased dramatically in the offspring heart under the action of PS-NPs. There was a meaningful sex × PS-NPs interaction ($P = 0.038$) and a meaningful main influence of PS-NPs ($P < 0.05$) and sex ($P < 0.05$) on cleaved caspase-3^{+} cells (Fig. 9C–D). Collectively, these results suggest that maternally consuming PS-NPs has different effects on heart cell apoptosis in male and female offspring.

4. Discussion

Plastic particles are pervasive in air, water, and food [52,53], leading to their inevitable ingestion by humans through various routes. There is increasing concern about the potential adverse effects of MPs and NPs on human health. In this study, we found that maternal exposure to PS-NPs via drinking water has detrimental effects on the hearts of mouse offspring, manifested through increased fibrosis and apoptosis, enhanced immune $CD68^{+}$ macrophage infiltration, and metabolic disruption. These effects can lead to sex-specific cardiovascular disease in the offspring. The key findings underpinning our conclusions are as follows: Firstly, maternal exposure to PS-NPs affects the birth weight of male and female offspring differently. Secondly, the cardiac transcriptomes of male and female offspring exhibit significant differences; specifically, maternal-derived PS-NPs alter the transcriptome composition in the hearts of the offspring, resulting in distinct differential genes, KEGG pathways, and GO terms. Consistent with previous reports [43,54], the transcriptional composition of organ tissues demonstrates sexually dimorphic variations. Finally, PS-NPs adversely impact the heart by modifying the expression levels of genes related to fibrosis, metabolism, immunity, and apoptosis in the offspring. Our study provides further evidence of the pronounced impact of maternal PS-NPs exposure on offspring health and elucidates the mechanisms by which maternal PS-NPs influence the development of heart disease in offspring.

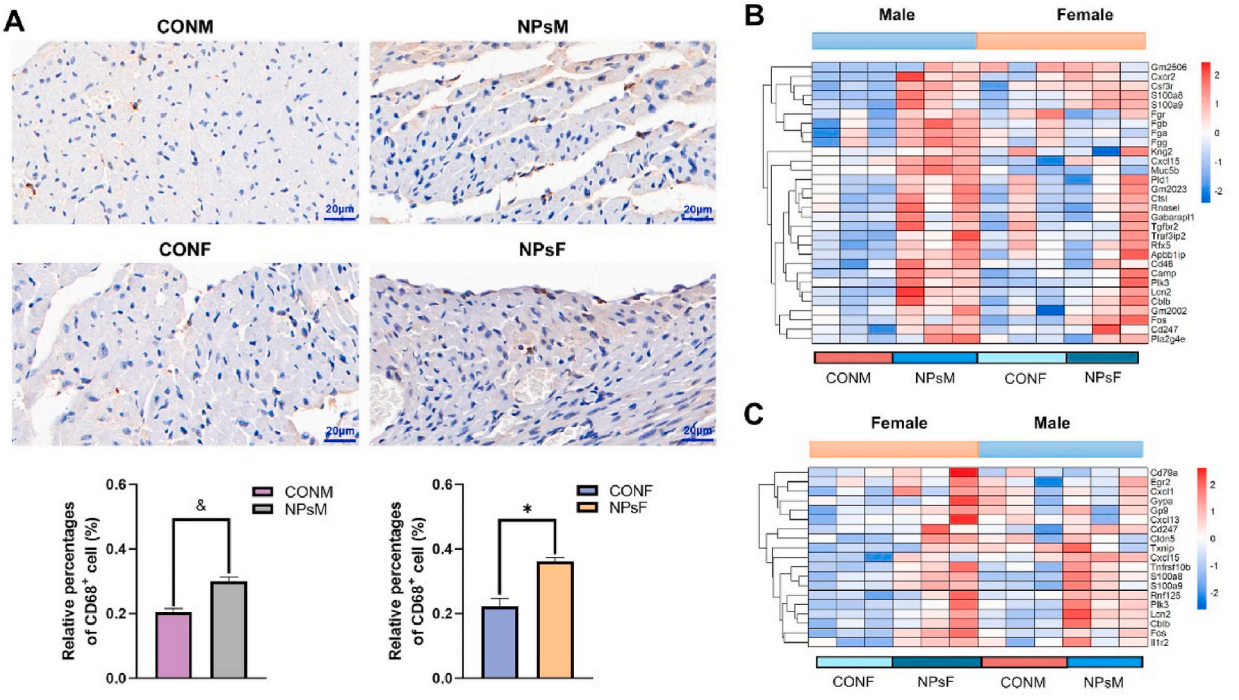

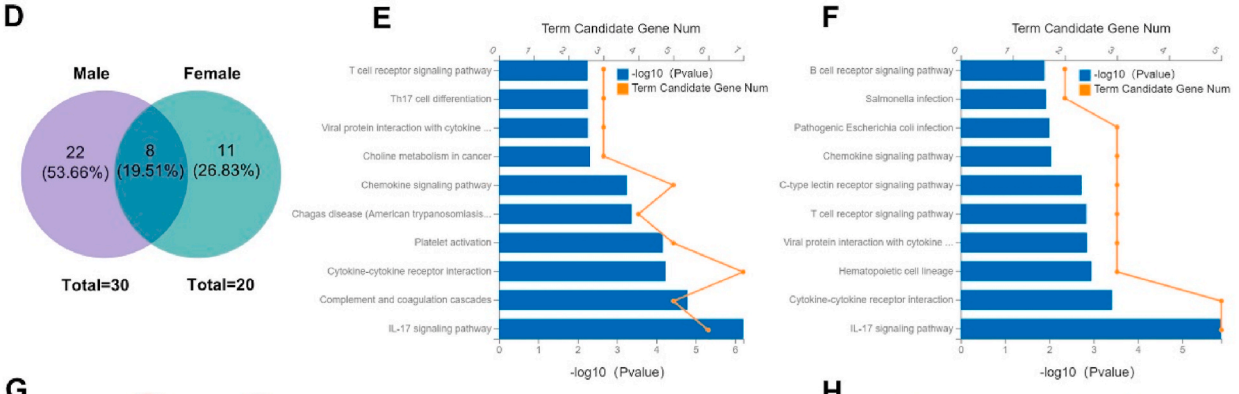

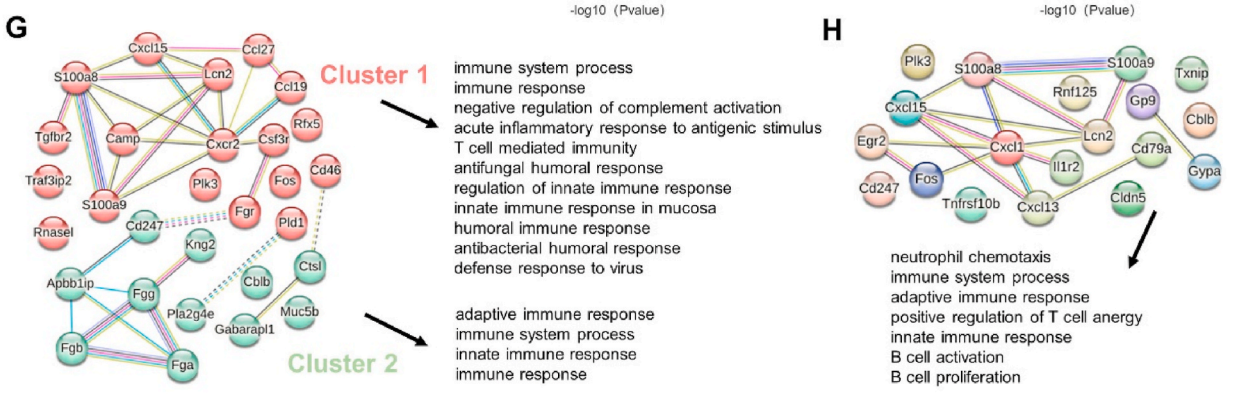

(caption on next page)

Fig. 8. PS-NPs alters the expression profile of genes associated with immunity in the heart of offspring. (A) Representative immunohistochemical images ($CD68^+$ macrophage) of normal heart and PS-NPs-treated heart in male and female offspring mice (N = 3 individual mice per group). The scale bar represents 50μm. $^{\&}P < 0.05$, $^{*}P < 0.05$. **(B–C)** Heatmaps of the immunity-associated genes in heart tissue of mice. Among, the male offspring mice ***(B)*** and the female offspring mice ***(C)***. The color bar indicates the scale used to show the expression of genes with the expression range normalized to ±2. **(D)** Venn diagram of significantly different genes related to immunity with NPsM and NPsF. **(E-F)** Gene annotation of KEGG pathways enriched in immunity-associated genes in heart tissue of the NPsM group ***(E)*** and the NPsF group ***(F)***, with $P < 0.05$. The top 10 pathways are shown. **(G-H)** The PPANs of the immunity-associated genes in heart of the NPsM group ***(G)*** and the NPsF group ***(H)***. Three mice in each group. (For interpretation of the references to color in this figure legend, the reader is referred to the Web version of this article.)

Perinatal maternal status has a profound impact on offspring health. It has been demonstrated that maternal diets high in fat, salt, sugar, and alcohol can adversely affect offspring health [55,56]. For example, reduced birth weight in offspring from high-fat diet pregnancies is associated with altered fetal growth rates, increased fat mass, and metabolic changes observed during weaning [55]. Furthermore, Perak et al. [57] reported a significant correlation between maternal cardiovascular health during gestation and the cardiovascular health of children in early adolescence. As society progresses, the likelihood of maternal exposure to adverse factors (such as maternal behaviors [58,59], and environmental toxins [60–62]) increases, which can profoundly impact offspring. Recent research by Wang et al. [60] demonstrated that PS-NPs induce a range of congenital malformations, including those affecting heart tissue. In this study, we exposed maternal mice to PS-NPs from pregnancy through three weeks postpartum. The observed increase in the HW/BW ratio in PS-NPs-exposed offspring, despite a reduction in heart weight, suggests a compensatory cardiac response to maternal exposure. This phenomenon likely results from a greater reduction in body mass, leading to a relatively increased HW/BW ratio. Such changes may reflect early cardiac remodeling processes, where the heart attempts to maintain functional output despite metabolic and growth challenges. The molecular disruptions identified in our transcriptomic analysis, particularly in pathways related to fibrosis, metabolism, and immune regulation, may contribute to this maladaptive remodeling. The overall reduction in heart weight across both sexes indicates that PS-NPs impede normal cardiac growth, possibly through nutrient or signaling impairments in utero. The pronounced effects on body weight exacerbate this imbalance, resulting in an elevated HW/BW ratio as the heart adapts to systemic stress. These findings underscore the necessity for further investigation into the long-term cardiovascular consequences of maternal PS-NPs exposure.

The observed increase in cardiomyocyte size in male offspring exposed to PS-NPs may result from sex-specific responses to environmental stressors, such as nanoplastic exposure, which could induce a compensatory hypertrophic response. Cardiomyocyte hypertrophy is a well-documented adaptive mechanism to increased cardiac workload or metabolic disruptions [63,64]. In males, this hypertrophic response may be driven by alterations in metabolic signaling pathways, such as those related to lipid metabolism or mitochondrial function, which have been shown to be differentially regulated between sexes [65,66]. The reprogramming of cardiac transcriptional profiles, as indicated by our RNA sequencing data, supports the idea that male offspring may have an enhanced susceptibility to hypertrophic stimuli, potentially due to upregulation of genes involved in fibrosis, immune responses, and growth factor signaling. This reprogramming may contribute to the remodeling process observed as cardiomyocyte enlargement. Additionally, increased fluid shear stress and enrichment of atherosclerosis pathways in male offspring could exert hemodynamic forces that further promote cardiomyocyte hypertrophy. This finding is consistent with previous research demonstrating that males are more prone to developing hypertrophic responses under stress [67].

Sexually dimorphic differences significantly influence the onset and progression of various diseases, including variations in morbidity rates, age of onset, and disease severity [68–70]. These differences also impact gene expression levels and genetic regulation across tissues and organs [71]. For instance, women exhibit higher rates of depression and Alzheimer's disease [72,73], while men have higher incidences of schizophrenia, Parkinson's disease, and colorectal cancer [74–76]. Furthermore, boys show a higher incidence of asthma during childhood, whereas girls experience a higher rate of new cases around adolescence [77]. Recently, Joseph et al. [68] reported that differences in brain gene activity contribute to variations in typical sexual behavior between male and female offspring mice. Similarly, Yuan et al. [78] found that genetic differences affect lifespan in a sex-specific manner. Additionally, studies on virus-induced lung damage repair in mice have elucidated mechanisms underlying sex differences in lung disease [79]. For example, male db/db mice on a high-salt diet exhibit higher levels of inflammatory cytokines and greater renal immune cell infiltration compared to females [80], highlighting the sexually dimorphic effects of a high-salt diet. Our study also revealed sex-specific variability in the effects of maternal exposure to PS-NPs, consistent with observations of non-gestational sex differences [43,81]. Notably, the offspring of female mice exhibited significantly greater weight loss compared to those of male mice, aligning with most research findings [23]. Additionally, sexually dimorphic differences were observed in cardiomyocyte size among offspring mice. These data contribute to our understanding of how maternal exposure to PS-NPs affects the heart in a sex-specific manner.

To date, there is a paucity of data on the effects of exposure to PS-NPs during pregnancy and its impact on the transcriptome of the heart. Existing studies have primarily focused on the effects of nutritional deficiencies and high androgen exposure during pregnancy on the offspring's transcriptome and sexual dimorphism [82,83]. In this study, we observed that maternal exposure to PS-NPs led to sex-specific effects on the heart transcriptome in both male and female offspring. PCA and volcano plot analysis revealed significant differences in the composition of the heart transcriptome and the number of DEGs, with these differences being more pronounced in the PS-NP-exposed group. The distribution of highly expressed genes varied between sexes, with the number of highly expressed genes specific to female offspring in the control group being approximately 1.4 times greater than in male offspring. Additionally, the highly expressed genes in both male and female offspring in the PS-NP treatment group exhibited distinct KEGG pathways and functional categories. Beyond these sex-specific effects, we also found that PS-NPs adversely affect the offspring's heart by enhancing fibrosis and apoptosis, increasing $CD68^+$ macrophage infiltration, and disrupting metabolism. These findings indicate that maternal PS-NP

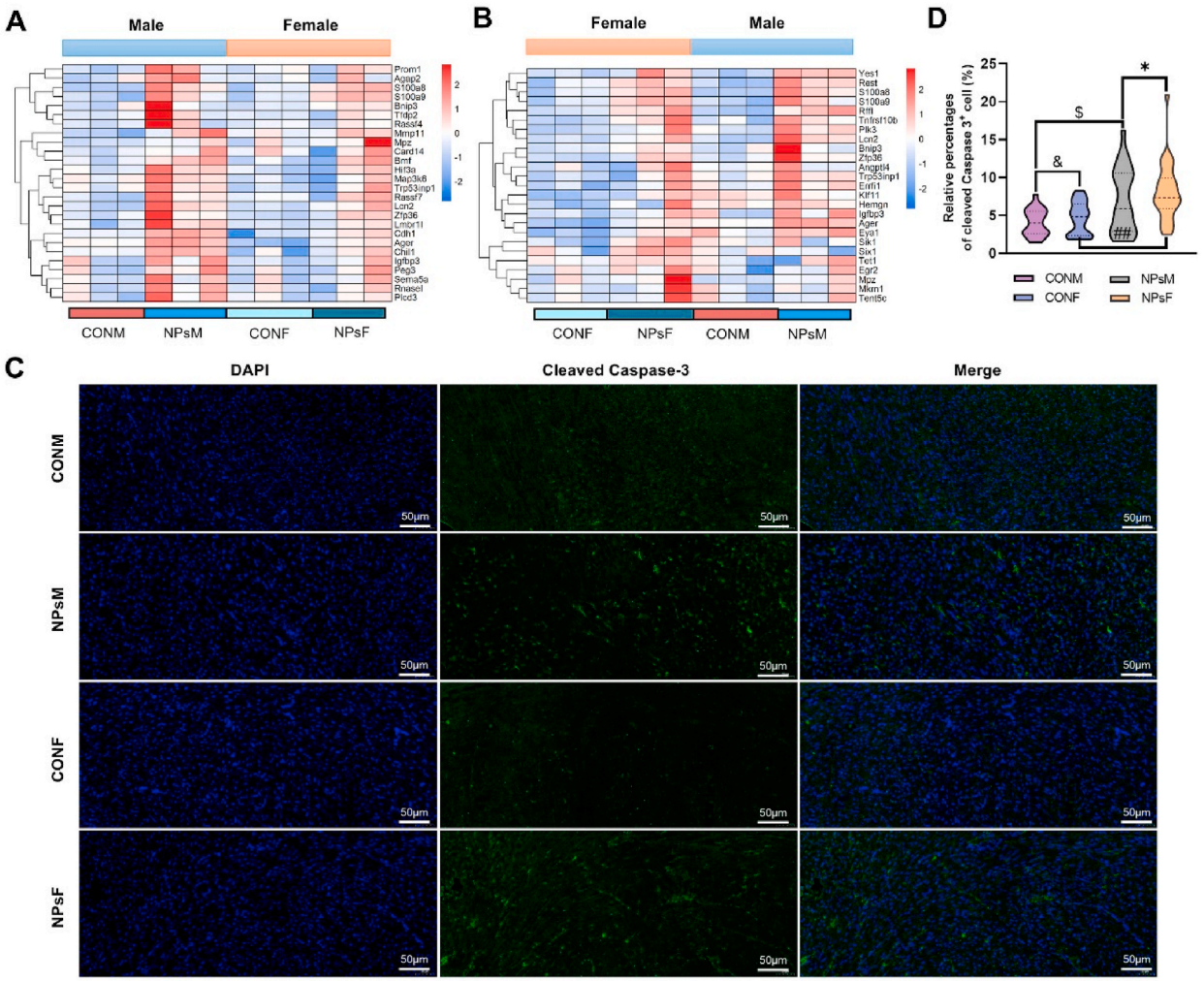

(caption on next page)

Fig. 9. The effect of PS-NPs on apoptosis in the offspring mice. (A–B) Heatmaps of genes associated with apoptosis in heart tissue of the offspring. Among, the NPsM group ***(A)*** and the NPsF group ***(B)***. The color bar indicates the scale used to show the expression of genes with the expression range normalized to ±2. (**C**) Representative immunofluorescent images (cleaved caspase-3) with CONM, NPsM, CONF, and NPsF. The scale bar represents 50 μm. (**D**) Average relative abundance of cleaved caspase-3^+ cells in the immunofluorescent images of cardiac sections from normal and PS-NPs-treated heart tissue in male mice and female mice. $^{*}P < 0.05$, $^{\$}P < 0.05$, $^{\&}P < 0.05$, $^{\#\#}P < 0.01$. N = 3 individual mice per group. (**E-F**) Gene annotation of molecular function and biological process of GO enriched terms for apoptosis-associated genes for heart tissue of mice, with $Q < 0.05$, the top 10 terms were shown. Among, the male offspring mice ***(E)*** and the female offspring mice ***(F)***. Three mice in each group. (For interpretation of the references to color in this figure legend, the reader is referred to the Web version of this article.)

exposure induces sex-specific changes in the transcriptomic profiles of the offspring's hearts.

Fibrosis can develop in a variety of organs [84], with myocardial fibrosis specifically referring to the loss of cardiac muscle elasticity in response to factors that damage cardiac cells [85,86]. This condition is often associated with increased cardiac volume and cardiomyocyte hypertrophy. Research has demonstrated that exposure to micro- and nanoplastics can induce cardiac fibrosis in mice and significantly alter the expression profile related to pulmonary fibrosis [22,87]. Building on these findings from studies on fibrosis in adult rats, and through the analysis of DEGs, KEGG pathways, GO molecular functions, biological functions, and pathological staining, our study reveals that maternal exposure to PS-NPs causes cardiac fibrosis in both male and female offspring. Notably, the degree of fibrosis was more pronounced in female offspring compared to their male counterparts.

Exposure to plastic products is closely associated with endocrine-related metabolic diseases and can impact early development [88]. Micro- and nano-plastics have been shown to increase the risk of cardiometabolic diseases, with potential effects lasting up to two generations [89,90]. Previous studies have demonstrated that maternal exposure to plastics can disrupt developmental processes, potentially leading to metabolic disorders in the offspring [91,92]. Additionally, Luo et al. [26] reported that maternal exposure to polystyrene microplastics of various sizes can induce metabolic disorders in offspring. In this study, we observed that maternal exposure to PS-NPs affects the expression profiles of metabolism-related genes in the offspring's heart. The impact is evident in the molecular biological processes identified through GO enrichment analysis, KEGG pathways, and the PPANs.

It is well-established that the ingestion of NPs can directly or indirectly affect the immune system, potentially leading to an imbalance in immune homeostasis [93–97]. In mice, oral administration of polyethylene NPs has been shown to significantly disrupt the intestinal microenvironment, triggering an adaptive immune response and promoting the growth of established colon tumors [94]. Li et al. [93] reported that PS-NPs could penetrate spleen lymphocytes and markedly reduce immune cell viability at high concentrations. Furthermore, Wang et al. [97] found that PS-NPs significantly altered the gut microbiome structure and gene expression related to the immune system, antioxidant responses, and detoxification processes, which contributed to host immune dysfunction. It has been demonstrated that maternal gut microbiota are closely linked to the immune system of the fetus or newborn [98], with maternal gut flora metabolites potentially affecting fetal immune system development through the placenta [99]. Our study indicates that maternal exposure to PS-NPs significantly altered the expression profiles of immune-related genes, immune-related KEGG pathways, and molecular biological processes in the hearts of both male and female offspring. Additionally, Baranzini et al. [100] showed that micro- and nanoplastics can induce an increase in $CD45^+$ and $CD68^+$ cells in Hirudo verbana. Moreover, increased infiltration of $CD45^+$ and $CD68^+$ cells has been observed in male rat heart tissue during the development of immunity [101]. Consistent with these findings, our study also demonstrates that maternal exposure to PS-NPs increases macrophage infiltration in the offspring's heart. This immune activation is primarily mediated by changes in macrophage activation states, promoting cell differentiation, and regulating the expression of inflammatory factors and genes [102]. Thus, the impact of maternal PS-NPs exposure on cardiac immunity and related effects in offspring may follow a similar pathway.

Apoptosis is a specific form of cell death that plays a crucial role in various heart-related pathologies, including heart hypertrophy and cardiac failure [101,103]. t has been reported that polystyrene microplastics accelerate myocardial cell apoptosis and induce myocardial fibrosis in rats through the activation of the Wnt/β-catenin pathway [104]. Early studies demonstrated that apoptosis is present during the morphogenesis and development of cardiac embryos, as observed in tests with chicken embryonic hearts. Additionally, apoptosis is increasingly recognized for its role in developmental signaling mechanisms [105,106]. For instance, caspase-3 knockout mice exhibit embryonic death on day 11 due to "myocardial damage." In our study, we found that maternal exposure to PS-NPs altered the expression of genes associated with apoptosis in the cardiac tissue of mouse offspring, with a more pronounced effect observed in females compared to males. Furthermore, PS-NPs significantly activated apoptosis and other molecular biological processes in offspring cardiac tissue, as indicated by GO analysis. However, the specific mechanism underlying PS-NPs-induced apoptosis in progeny cardiomyocytes warrants further investigation.

While our data demonstrate that maternal exposure to PS-NPs adversely affects cardiac gene expression in offspring mice, there are several limitations to this study. First, only C57BL/6J mice were used, and other animal models were not explored. Additionally, the impact of maternal PS-NPs exposure on cardiac development postnatally and the progression of heart-related diseases in adulthood require further investigation. Second, this study primarily focuses on transcriptomic analyses; thus, additional research is needed to examine the effects of maternal PS-NPs exposure on offspring metabolites and proteomics. Finally, a notable difference between mice and humans in the established murine model is that mice are nocturnal, which may influence the generalizability of the findings to human health. In conclusion, the clinical relevance of the results should be considered with caution. Further research is needed to elucidate the underlying mechanisms and assess the long-term effects.

5. Conclusion

In conclusion, our results suggest that maternal exposure to PS-NPs induces cardiotoxicity in offspring with sexually dimorphic effects, with female offspring exhibiting greater sensitivity than their male counterparts. Maternal exposure to PS-NPs significantly induces cardiac damage by altering metabolic, immune, fibrotic, and apoptotic processes in both male and female offspring. Maternal exposure to micro- and nanoplastics has adverse effects on the developing fetus. Therefore, considering the interactions between sex-specific genes and maternal factors, maternal PS-NPs-induced cardiac programming provides theoretical support for evaluating potential gender-specific clinical risks, understanding the pathogenesis of cardiac damage, and developing therapeutic interventions.

CRediT authorship contribution statement

Xiuli Chen: Writing – review & editing, Writing – original draft, Methodology, Investigation, Funding acquisition, Data curation. **Shenzhen Huang:** Writing – review & editing, Writing – original draft, Investigation, Funding acquisition, Conceptualization. **Li Wang:** Investigation, Data curation. **Kan Liu:** Investigation, Data curation. **Haiying Wu:** Writing – review & editing, Resources, Conceptualization.

Declaration of competing interest

The authors declare that they have no known competing financial interests or personal relationships that could have appeared to influence the work reported in this paper.

Acknowledgments

This work was supported by the Natural Science Foundation of Henan (grant number 222300420361, X.C.), the Henan Science and Technology R&D Program Joint Fund Project (grant numbers 235200810064, X.C. and 242102311128, H. W.), the Henan Provincial Medical Science and Technology Research Joint Co-construction Project (grant number LHGJ20220054, X.C.), and the Provincial and Ministry Co-constructed Key Projects of Henan Provincial Health Commission (grant number SBGJ202302098, S.H.).

Appendix A. Supplementary data

Supplementary data to this article can be found online at https://doi.org/10.1016/j.heliyon.2024.e39139.

References

[1] A. Ragusa, A. Svelato, C. Santacroce, P. Catalano, V. Notarstefano, O. Carnevali, F. Papa, M.C.A. Rongioletti, F. Baiocco, S. Draghi, E. D'Amore, D. Rinaldo, M. Matta, E. Giorgini, Plasticenta: first evidence of microplastics in human placenta, Environ. Int. 146 (2021) 106274. https://doi:10.1016/j.envint.2020.106274.

[2] P. Schwabl, S. Köppel, P. Königshofer, T. Bucsics, M. Trauner, T. Reiberger, B. Liebmann, Detection of various microplastics in human stool: a prospective case series, Ann. Intern. Med. 171 (2019) 453–457. https://doi:10.7326/m19-0618.

[3] H.A. Leslie, M.J.M. van Velzen, S.H. Brandsma, A.D. Vethaak, J.J. Garcia-Vallejo, M.H. Lamoree, Discovery and quantification of plastic particle pollution in human blood, Environ. Int. 163 (2022) 107199. https://doi:10.1016/j.envint.2022.107199.

[4] A. Ragusa, V. Notarstefano, A. Svelato, A. Belloni, G. Gioacchini, C. Blondeel, E. Zucchelli, C. De Luca, S. D'Avino, A. Gulotta, O. Carnevali, E. Giorgini, Raman microspectroscopy detection and characterisation of microplastics in human breastmilk, Polymers 14 (2022). https://doi:10.3390/polym14132700.

[5] T. Horvatits, M. Tamminga, B. Liu, M. Sebode, A. Carambia, L. Fischer, K. Püschel, S. Huber, E.K. Fischer, Microplastics detected in cirrhotic liver tissue, EBioMedicine 82 (2022) 104147. https://doi:10.1016/j.ebiom.2022.104147.

[6] L.C. Jenner, J.M. Rotchell, R.T. Bennett, M. Cowen, V. Tentzeris, L.R. Sadofsky, Detection of microplastics in human lung tissue using μFTIR spectroscopy, Sci. Total Environ. 831 (2022) 154907. https://doi:10.1016/j.scitotenv.2022.154907.

[7] J. Brahney, M. Hallerud, E. Heim, M. Hahnenberger, S. Sukumaran, Plastic rain in protected areas of the United States, Science 368 (2020) 1257–1260. https://doi:10.1126/science.aaz5819.

[8] M.L. Rivas, I. Albion, B. Bernal, R.N. Handcock, S.J. Heatwole, M.L. Parrott, K.A. Piazza, E. Deschaseaux, The plastic pandemic: COVID-19 has accelerated plastic pollution, but there is a cure, Sci. Total Environ. 847 (2022) 157555. https://doi:10.1016/j.scitotenv.2022.157555.

[9] A.L. Andrady, The plastic in microplastics: a review, Mar. Pollut. Bull. 119 (2017) 12–22. https://doi:10.1016/j.marpolbul.2017.01.082.

[10] Y.K. Song, S.H. Hong, M. Jang, G.M. Han, S.W. Jung, W.J. Shim, Combined effects of UV exposure duration and mechanical abrasion on microplastic fragmentation by polymer type, Environ. Sci. Technol. 51 (2017) 4368–4376. https://doi:10.1021/acs.est.6b06155.

[11] J. Gigault, A.T. Halle, M. Baudrimont, P.Y. Pascal, F. Gauffre, T.L. Phi, H. El Hadri, B. Grassl, S. Reynaud, Current opinion: what is a nanoplastic? Environ Pollut 235 (2018) 1030–1034. https://doi:10.1016/j.envpol.2018.01.024.

[12] R. Lehner, C. Weder, A. Petri-Fink, B. Rothen-Rutishauser, Emergence of nanoplastic in the environment and possible impact on human health, Environ. Sci. Technol. 53 (2019) 1748–1765. https://doi:10.1021/acs.est.8b05512.

[13] M. Zatorska-Płachta, G. Łazarski, U. Maziarz, A. Foryś, B. Trzebicka, D. Wnuk, K. Chołuj, A. Karewicz, M. Michalik, D. Jamróz, M. Kepczynski, Encapsulation of curcumin in polystyrene-based nanoparticles-drug loading capacity and cytotoxicity, ACS Omega 6 (2021) 12168–12178. https://doi:10.1021/acsomega.1c00867.

[14] V. Kopatz, K. Wen, T. Kovács, A.S. Keimowitz, V. Pichler, J. Widder, A.D. Vethaak, O. Hollóczki, L. Kenner, Micro- and nanoplastics breach the blood-brain barrier (BBB): biomolecular corona's role revealed, Nanomaterials 13 (2023). https://doi:10.3390/nano13081404.

[15] S. Liu, Y. Li, L. Shang, J. Yin, Z. Qian, C. Chen, Y. Yang, Size-dependent neurotoxicity of micro- and nanoplastics in flowing condition based on an in vitro microfluidic study, Chemosphere 303 (2022) 135280. https://doi:10.1016/j.chemosphere.2022.135280.

[16] K. Kik, B. Bukowska, P. Sicińska, Polystyrene nanoparticles: sources, occurrence in the environment, distribution in tissues, accumulation and toxicity to various organisms, Environ Pollut 262 (2020) 114297. https://doi:10.1016/j.envpol.2020.114297.

[17] L. Liu, K. Xu, B. Zhang, Y. Ye, Q. Zhang, W. Jiang, Cellular internalization and release of polystyrene microplastics and nanoplastics, Sci. Total Environ. 779 (2021) 146523. https://doi:10.1016/j.scitotenv.2021.146523.

[18] W. Zhou, D. Tong, D. Tian, Y. Yu, L. Huang, W. Zhang, Y. Yu, L. Lu, X. Zhang, W. Pan, J. Shen, W. Shi, G. Liu, Exposure to polystyrene nanoplastics led to learning and memory deficits in zebrafish by inducing oxidative damage and aggravating brain aging, Adv Healthc Mater 12 (2023) e2301799. https://doi:10.1002/adhm.202301799.

[19] L. Miao, S. Guo, J. Wu, T.M. Adyel, Z. Liu, S. Liu, J. Hou, Polystyrene nanoplastics change the functional traits of biofilm communities in freshwater environment revealed by GeoChip 5.0, J. Hazard Mater. 423 (2022) 127117. https://doi:10.1016/j.jhazmat.2021.127117.

[20] S. Shan, Y. Zhang, H. Zhao, T. Zeng, X. Zhao, Polystyrene nanoplastics penetrate across the blood-brain barrier and induce activation of microglia in the brain of mice, Chemosphere 298 (2022) 134261. https://doi:10.1016/j.chemosphere.2022.134261.

[21] Y. He, Z. Li, T. Xu, D. Luo, Q. Chi, Y. Zhang, S. Li, Polystyrene nanoplastics deteriorate LPS-modulated duodenal permeability and inflammation in mice via ROS drived-NF-κB/NLRP3 pathway, Chemosphere 307 (2022) 135662. https://doi:10.1016/j.chemosphere.2022.135662.

[22] P. Lin, X. Tong, F. Xue, C. Qianru, T. Xinyu, L. Zhe, B. Zhikun, L. Shu, Polystyrene nanoplastics exacerbate lipopolysaccharide-induced myocardial fibrosis and autophagy in mice via ROS/TGF-β1/Smad, Toxicology 480 (2022) 153338. https://doi:10.1016/j.tox.2022.153338.

[23] J. Tang, W. Bu, W. Hu, Z. Zhao, L. Liu, C. Luo, R. Wang, S. Fan, S. Yu, Q. Wu, X. Wang, X. Zhao, Ferroptosis is involved in sex-specific small intestinal toxicity in the offspring of adult mice exposed to polystyrene nanoplastics during pregnancy, ACS Nano 17 (2023) 2440–2449. https://doi:10.1021/acsnano.2c09729.

[24] Q. Guo, Y. Tang, Y. Li, Z. Xu, D. Zhang, J. Liu, X. Wang, W. Xia, S. Xu, Perinatal high-salt diet induces gut microbiota dysbiosis, bile acid homeostasis disbalance, and NAFLD in weanling mice offspring, Nutrients 13 (2021). https://doi:10.3390/nu13072135.

[25] C.C. Wong, A. Caspi, B. Williams, I.W. Craig, R. Houts, A. Ambler, T.E. Moffitt, J. Mill, A longitudinal study of epigenetic variation in twins, Epigenetics 5 (2010) 516–526. https://doi:10.4161/epi.5.6.12226.

[26] T. Luo, Y. Zhang, C. Wang, X. Wang, J. Zhou, M. Shen, Y. Zhao, Z. Fu, Y. Jin, Maternal exposure to different sizes of polystyrene microplastics during gestation causes metabolic disorders in their offspring, Environ Pollut 255 (2019) 113122. https://doi:10.1016/j.envpol.2019.113122.

[27] Q. Yang, H. Dai, Y. Cheng, B. Wang, J. Xu, Y. Zhang, Y. Chen, F. Xu, Q. Ma, F. Lin, C. Wang, Oral feeding of nanoplastics affects brain function of mice by inducing macrophage IL-1 signal in the intestine, Cell Rep. 42 (2023) 112346. https://doi:10.1016/j.celrep.2023.112346.

[28] D. Yang, J. Zhu, X. Zhou, D. Pan, S. Nan, R. Yin, Q. Lei, N. Ma, H. Zhu, J. Chen, L. Han, M. Ding, Y. Ding, Polystyrene micro- and nano-particle coexposure injures fetal thalamus by inducing ROS-mediated cell apoptosis, Environ. Int. 166 (2022) 107362. https://doi:10.1016/j.envint.2022.107362.

[29] V. Tanwar, J.M. Adelstein, J.A. Grimmer, D.J. Youtz, B.P. Sugar, L.E. Wold, PM(2.5) exposure in utero contributes to neonatal cardiac dysfunction in mice, Environ Pollut 230 (2017) 116–124. https://doi:10.1016/j.envpol.2017.06.035.

[30] Q.A. Hathaway, C.E. Nichols, D.L. Shepherd, P.A. Stapleton, S.L. McLaughlin, J.C. Stricker, S.L. Rellick, M.V. Pinti, A.B. Abukabda, C.R. McBride, J. Yi, S. M. Stine, T.R. Nurkiewicz, J.M. Hollander, Maternal-engineered nanomaterial exposure disrupts progeny cardiac function and bioenergetics, Am. J. Physiol. Heart Circ. Physiol. 312 (2017) H446–h458. https://doi:10.1152/ajpheart.00634.2016.

[31] S. Bojic, M.M. Falco, P. Stojkovic, B. Ljujic, M. Gazdic Jankovic, L. Armstrong, N. Markovic, J. Dopazo, M. Lako, R. Bauer, M. Stojkovic, Platform to study intracellular polystyrene nanoplastic pollution and clinical outcomes, Stem Cell. 38 (2020) 1321–1325. https://doi:10.1002/stem.3244.

[32] E.A. Melnik, Y.P. Buzulukov, V.F. Demin, V.A. Demin, I.V. Gmoshinski, N.V. Tyshko, V.A. Tutelyan, Transfer of silver nanoparticles through the placenta and breast milk during in vivo experiments on rats, Acta Naturae 5 (2013) 107–115.

[33] S.A. Byron, K.R. Van Keuren-Jensen, D.M. Engelthaler, J.D. Carpten, D.W. Craig, Translating RNA sequencing into clinical diagnostics: opportunities and challenges, Nat. Rev. Genet. 17 (2016) 257–271. https://doi:10.1038/nrg.2016.10.

[34] T. Huang, W. Zhang, T. Lin, S. Liu, Z. Sun, F. Liu, Y. Yuan, X. Xiang, H. Kuang, B. Yang, D. Zhang, Maternal exposure to polystyrene nanoplastics during gestation and lactation induces hepatic and testicular toxicity in male mouse offspring, Food Chem. Toxicol. 160 (2022) 112803. https://doi:10.1016/j.fct.2021.112803.

[35] G. Chen, S. Xiong, Q. Jing, C.A.M. van Gestel, N.M. van Straalen, D. Roelofs, L. Sun, H. Qiu, Maternal exposure to polystyrene nanoparticles retarded fetal growth and triggered metabolic disorders of placenta and fetus in mice, Sci. Total Environ. 854 (2023) 158666. https://doi:10.1016/j.scitotenv.2022.158666.

[36] X. Fan, X. Wei, H. Hu, B. Zhang, D. Yang, H. Du, R. Zhu, X. Sun, Y. Oh, N. Gu, Effects of oral administration of polystyrene nanoplastics on plasma glucose metabolism in mice, Chemosphere 288 (2022) 132607. https://doi:10.1016/j.chemosphere.2021.132607.

[37] S.B. Fournier, J.N. D'Errico, D.S. Adler, S. Kollontzi, M.J. Goedken, L. Fabris, E.J. Yurkow, P.A. Stapleton, Nanopolystyrene translocation and fetal deposition after acute lung exposure during late-stage pregnancy, Part. Fibre Toxicol. 17 (2020) 55. https://doi:10.1186/s12989-020-00385-9.

[38] F. Mao, E. Wang, J. Xu, J. Lu, G. Yan, L. Fu, Y. Jiao, L. Wu, T. Liu, Y. Li, Transcriptome analysis of multiple metabolic tissues in high-salt diet-fed mice, Front. Endocrinol. 13 (2022) 887843. https://doi:10.3389/fendo.2022.887843.

[39] D.W. Ho, Z.F. Yang, K. Yi, C.T. Lam, M.N. Ng, W.C. Yu, J. Lau, T. Wan, X. Wang, Z. Yan, H. Liu, Y. Zhang, S.T. Fan, Gene expression profiling of liver cancer stem cells by RNA-sequencing, PLoS One 7 (2012) e37159. https://doi:10.1371/journal.pone.0037159.

[40] M.E. Sweet, A. Cocciolo, D. Slavov, K.L. Jones, J.R. Sweet, S.L. Graw, T.B. Reece, A.V. Ambardekar, M.R. Bristow, L. Mestroni, M.R.G. Taylor, Transcriptome analysis of human heart failure reveals dysregulated cell adhesion in dilated cardiomyopathy and activated immune pathways in ischemic heart failure, BMC Genom. 19 (2018) 812. https://doi:10.1186/s12864-018-5213-9.

[41] A. Conesa, P. Madrigal, S. Tarazona, D. Gomez-Cabrero, A. Cervera, A. McPherson, M.W. Szcześniak, D.J. Gaffney, L.L. Elo, X. Zhang, A. Mortazavi, A survey of best practices for RNA-seq data analysis, Genome Biol. 17 (2016) 13. https://doi:10.1186/s13059-016-0881-8.

[42] E.F. Trakhtenberg, N. Pho, K.M. Holton, T.W. Chittenden, J.L. Goldberg, L. Dong, Cell types differ in global coordination of splicing and proportion of highly expressed genes, Sci. Rep. 6 (2016) 32249. https://doi:10.1038/srep32249.

[43] X. Chen, H. Wu, S. Huang, Excessive sodium intake leads to cardiovascular disease by promoting sex-specific dysfunction of murine heart, Front. Nutr. 9 (2022) 830738. https://doi:10.3389/fnut.2022.830738.

[44] H. Dong, Y. Xia, S. Jin, C. Xue, Y. Wang, R. Hu, H. Jiang, Nrf2 attenuates ferroptosis-mediated IIR-ALI by modulating TERT and SLC7A11, Cell Death Dis. 12 (2021) 1027. https://doi:10.1038/s41419-021-04307-1.

[45] Y. Zhao, X.Q. Wang, R.Q. Liu, F.W. Jiang, J.X. Wang, M.S. Chen, H. Zhang, J.G. Cui, Y.H. Chang, J.L. Li, SLC7A11 as a therapeutic target to attenuate phthalates-driven testosterone level decline in mice, J. Adv. Res. (2024). https://doi:10.1016/j.jare.2024.05.026 (in press).

[46] D. Liu, Q. Ding, D.F. Dai, B. Padhy, M.K. Nayak, C. Li, M. Purvis, H. Jin, C. Shu, A.K. Chauhan, C.L. Huang, M. Attanasio, Loss of diacylglycerol kinase ε causes thrombotic microangiopathy by impairing endothelial VEGFA signaling, JCI Insight 6 (2021). https://doi:10.1172/jci.insight.146959.

[47] É. Szentirmai, L. Kapás, The role of the brown adipose tissue in β3-adrenergic receptor activation-induced sleep, metabolic and feeding responses, Sci. Rep. 7 (2017) 958. https://doi:10.1038/s41598-017-01047-1.

[48] D. Szklarczyk, A.L. Gable, D. Lyon, A. Junge, S. Wyder, J. Huerta-Cepas, M. Simonovic, N.T. Doncheva, J.H. Morris, P. Bork, L.J. Jensen, C.V. Mering, STRING v11: protein-protein association networks with increased coverage, supporting functional discovery in genome-wide experimental datasets, Nucleic Acids Res. 47 (2019) D607–d613. https://doi:10.1093/nar/gky1131.

[49] M.S. DeRycke, J.D. Andersen, K.M. Harrington, S.E. Pambuccian, S.E. Kalloger, K.L. Boylan, P.A. Argenta, A.P. Skubitz, S100A1 expression in ovarian and endometrial endometrioid carcinomas is a prognostic indicator of relapse-free survival, Am. J. Clin. Pathol. 132 (2009) 846–856. https://doi:10.1309/ajcptk87emmikpfs.

[50] S. Yuan, C. Wei, G. Liu, L. Zhang, J. Li, L. Li, S. Cai, L. Fang, Sorafenib attenuates liver fibrosis by triggering hepatic stellate cell ferroptosis via HIF-1α/SLC7A11 pathway, Cell Prolif. 55 (2022) e13158. https://doi:10.1111/cpr.13158.

[51] Y. Feng, W. Li, Z. Wang, R. Zhang, Y. Li, L. Zang, P. Wang, Z. Li, Y. Dong, The p-STAT3/ANXA2 axis promotes caspase-1-mediated hepatocyte pyroptosis in non-alcoholic steatohepatitis, J. Transl. Med. 20 (2022) 497. https://doi:10.1186/s12967-022-03692-1.

[52] Q. Liu, Z. Chen, Y. Chen, F. Yang, W. Yao, Y. Xie, Microplastics and nanoplastics: emerging contaminants in food, J. Agric. Food Chem. 69 (2021) 10450–10468. https://doi:10.1021/acs.jafc.1c04199.

[53] D. Allen, S. Allen, S. Abbasi, A. Baker, M. Bergmann, J. Brahney, T. Butler, R.A. Duce, S. Eckhardt, N. Evangeliou, T. Jickells, M. Kanakidou, P. Kershaw, P. Laj, J. Levermore, D. Li, P. Liss, K. Liu, N. Mahowald, P. Masque, D. Materić, A.G. Mayes, P. McGinnity, I. Osvath, K.A. Prather, J.M. Prospero, L.E. Revell, S. G. Sander, W.J. Shim, J. Slade, A. Stein, O. Tarasova, S. Wright, Microplastics and nanoplastics in the marine-atmosphere environment, Nat. Rev. Earth Environ. 3 (2022) 393–405. https://doi:10.1038/s43017-022-00292-x.

[54] F. Simunovic, M. Yi, Y. Wang, R. Stephens, K.C. Sonntag, Evidence for gender-specific transcriptional profiles of nigral dopamine neurons in Parkinson disease, PLoS One 5 (2010) e8856. https://doi:10.1371/journal.pone.0008856.

[55] C.M. Reynolds, M.H. Vickers, C.J. Harrison, S.A. Segovia, C. Gray, High fat and/or high salt intake during pregnancy alters maternal meta-inflammation and offspring growth and metabolic profiles, Physiol Rep 2 (2014). https://doi:10.14814/phy2.12110.

[56] K.D. MacDonald, A.R. Moran, A.J. Scherman, C.T. McEvoy, A.S. Platteau, Maternal high-fat diet in mice leads to innate airway hyperresponsiveness in the adult offspring, Physiol Rep 5 (2017). https://doi:10.14814/phy2.13082.

[57] A.M. Perak, N. Lancki, A. Kuang, D.R. Labarthe, N.B. Allen, S.H. Shah, L.P. Lowe, W.A. Grobman, J.M. Lawrence, D.M. Lloyd-Jones, W.L. Lowe Jr., D. M. Scholtens, Associations of maternal cardiovascular health in pregnancy with offspring cardiovascular health in early adolescence, JAMA 325 (2021) 658–668. https://doi:10.1001/jama.2021.0247.

[58] K. Agarwal, P. Manza, H.A. Tejeda, A.B. Courville, N.D. Volkow, P.V. Joseph, Prenatal caffeine exposure is linked to elevated sugar intake and BMI, altered reward sensitivity, and aberrant insular thickness in adolescents: an ABCD investigation, Nutrients 14 (2022). https://doi:10.3390/nu14214643.

[59] L. Han, C. Ren, L. Li, X. Li, J. Ge, H. Wang, Y.L. Miao, X. Guo, K.H. Moley, W. Shu, Q. Wang, Embryonic defects induced by maternal obesity in mice derive from Stella insufficiency in oocytes, Nat. Genet. 50 (2018) 432–442. https://doi:10.1038/s41588-018-0055-6.

[60] M. Wang, M. Rücklin, R.E. Poelmann, C.L. de Mooij, M. Fokkema, G.E.M. Lamers, M.A.G. de Bakker, E. Chin, L.J. Bakos, F. Marone, B.J. Wisse, M.C. de Ruiter, S. Cheng, L. Nurhidayat, M.G. Vijver, M.K. Richardson, Nanoplastics causes extensive congenital malformations during embryonic development by passively targeting neural crest cells, Environ. Int. 173 (2023) 107865. https://doi:10.1016/j.envint.2023.107865.

[61] A.K. Bozack, S.L. Rifas-Shiman, B.A. Coull, A.A. Baccarelli, R.O. Wright, C. Amarasiriwardena, D.R. Gold, E. Oken, M.F. Hivert, A. Cardenas, Prenatal metal exposure, cord blood DNA methylation and persistence in childhood: an epigenome-wide association study of 12 metals, Clin Epigenetics 13 (2021) 208. https://doi:10.1186/s13148-021-01198-z.

[62] V. Midya, E. Colicino, D.V. Conti, K. Berhane, E. Garcia, N. Stratakis, S. Andrusaityte, X. Basagaña, M. Casas, S. Fossati, R. Gražuleviciene, L.S. Haug, B. Heude, L. Maitre, R. McEachan, E. Papadopoulou, T. Roumeliotaki, C. Philippat, C. Thomsen, J. Urquiza, M. Vafeiadi, N. Varo, M.B. Vos, J. Wright, R. McConnell, M. Vrijheid, L. Chatzi, D. Valvi, Association of prenatal exposure to endocrine-disrupting chemicals with liver injury in children, JAMA Netw. Open 5 (2022) e2220176. https://doi:10.1001/jamanetworkopen.2022.20176.

[63] J. Ritterhoff, R. Tian, Metabolic mechanisms in physiological and pathological cardiac hypertrophy: new paradigms and challenges, Nat. Rev. Cardiol. 20 (2023) 812–829. https://doi:10.1038/s41569-023-00887-x.

[64] B. Crozatier, R. Ventura-Clapier, Inhibition of hypertrophy, per se, may not be a good therapeutic strategy in ventricular pressure overload: other approaches could be more beneficial, Circulation 131 (2015) 1448–1457. https://doi:10.1161/circulationaha.114.013895.

[65] Y. Cao, L. Vergnes, Y.C. Wang, C. Pan, K. Chella Krishnan, T.M. Moore, M. Rosa-Garrido, T.H. Kimball, Z. Zhou, S. Charugundla, C.D. Rau, M.M. Seldin, J. Wang, Y. Wang, T.M. Vondriska, K. Reue, A.J. Lusis, Sex differences in heart mitochondria regulate diastolic dysfunction, Nat. Commun. 13 (2022) 3850. https://doi:10.1038/s41467-022-31544-5.

[66] E. Murphy, G. Amanakis, N. Fillmore, R.J. Parks, J. Sun, Sex differences in metabolic cardiomyopathy, Cardiovasc. Res. 113 (2017) 370–377. https://doi:10.1093/cvr/cvx008.

[67] T.G. Martin, L.A. Leinwand, Hearts apart: sex differences in cardiac remodeling in health and disease, J. Clin. Invest. 134 (2024). https://doi:10.1172/jci180074.

[68] J.R. Knoedler, S. Inoue, D.W. Bayless, T. Yang, A. Tantry, C.H. Davis, N.Y. Leung, S. Parthasarathy, G. Wang, M. Alvarado, A.H. Rizvi, L.E. Fenno, C. Ramakrishnan, K. Deisseroth, N.M. Shah, A functional cellular framework for sex and estrous cycle-dependent gene expression and behavior, Cell 185 (2022) 654–671.e622. https://doi:10.1016/j.cell.2021.12.031.

[69] C. Ober, D.A. Loisel, Y. Gilad, Sex-specific genetic architecture of human disease, Nat. Rev. Genet. 9 (2008) 911–922. https://doi:10.1038/nrg2415.

[70] H.M. Edwards, C.E. Wallace, W.D. Gardiner, B.M. Doherty, R.T. Harrigan, K.M. Yuede, C.M. Yuede, J.R. Cirrito, Sex-dependent effects of acute stress on amyloid-β in male and female mice, Brain 146 (2023) 2268–2274. https://doi:10.1093/brain/awad052.

[71] M. Oliva, M. Muñoz-Aguirre, S. Kim-Hellmuth, V. Wucher, A.D.H. Gewirtz, D.J. Cotter, P. Parsana, S. Kasela, B. Balliu, A. Viñuela, S.E. Castel, P. Mohammadi, F. Aguet, Y. Zou, E.A. Khramtsova, A.D. Skol, D. Garrido-Martín, F. Reverter, A. Brown, P. Evans, E.R. Gamazon, A. Payne, R. Bonazzola, A.N. Barbeira, A. R. Hamel, A. Martinez-Perez, J.M. Soria, B.L. Pierce, M. Stephens, E. Eskin, E.T. Dermitzakis, A.V. Segrè, H.K. Im, B.E. Engelhardt, K.G. Ardlie, S. B. Montgomery, A.J. Battle, T. Lappalainen, R. Guigó, B.E. Stranger, The impact of sex on gene expression across human tissues, Science 369 (2020). https://doi:10.1126/science.aba3066.

[72] Y. Yan, S. Dominguez, D.W. Fisher, H. Dong, Sex differences in chronic stress responses and Alzheimer's disease, Neurobiol Stress 8 (2018) 120–126. https://doi:10.1016/j.ynstr.2018.03.002.

[73] Global prevalence and burden of depressive and anxiety disorders in 204 countries and territories in 2020 due to the COVID-19 pandemic, Lancet 398 (2021) 1700–1712. https://doi:10.1016/s0140-6736(21)02143-7.

[74] A. Aleman, R.S. Kahn, J.P. Selten, Sex differences in the risk of schizophrenia: evidence from meta-analysis, Arch Gen Psychiatry 60 (2003) 565–571. https://doi:10.1001/archpsyc.60.6.565.

[75] G. Matanoski, X. Tao, L. Almon, A.A. Adade, J.O. Davies-Cole, Demographics and tumor characteristics of colorectal cancers in the United States, 1998-2001, Cancer 107 (2006) 1112–1120. https://doi:10.1002/cncr.22008.

[76] G.F. Wooten, L.J. Currie, V.E. Bovbjerg, J.K. Lee, J. Patrie, Are men at greater risk for Parkinson's disease than women? J. Neurol. Neurosurg. Psychiatry 75 (2004) 637–639. https://doi:10.1136/jnnp.2003.020982.

[77] D.S. Postma, Gender differences in asthma development and progression, Gend. Med. 4 (Suppl B) (2007) S133–S146. https://doi:10.1016/s1550-8579(07)80054-4.

[78] R. Yuan, C.J.M. Musters, Y. Zhu, T.R. Evans, Y. Sun, E.J. Chesler, L.L. Peters, D.E. Harrison, A. Bartke, Genetic differences and longevity-related phenotypes influence lifespan and lifespan variation in a sex-specific manner in mice, Aging Cell 19 (2020) e13263. https://doi:10.1111/acel.13263.

[79] I. Sierra, S. Pyfrom, A. Weiner, G. Zhao, A. Driscoll, X. Yu, B.D. Gregory, A.E. Vaughan, M.C. Anguera, Unusual X chromosome inactivation maintenance in female alveolar type 2 cells is correlated with increased numbers of X-linked escape genes and sex-biased gene expression, Stem Cell Rep. 18 (2023) 489–502. https://doi:10.1016/j.stemcr.2022.12.005.

[80] L.C. Veiras, J.Z.Y. Shen, E.A. Bernstein, G.C. Regis, D. Cao, D. Okwan-Duodu, Z. Khan, D.R. Gibb, F.P. Dominici, K.E. Bernstein, J.F. Giani, Renal inflammation induces salt sensitivity in male db/db mice through dysregulation of ENaC, J. Am. Soc. Nephrol. 32 (2021) 1131–1149. https://doi:10.1681/asn.2020081112.

[81] X. Wang, Z. Zhao, X. Wang, W. Hu, L. Chao, X. Chu, M. Qian, R. Wang, S. Yu, Q. Wu, J. Tang, X. Zhao, Effects of polystyrene nanoplastic gestational exposure on mice, Chemosphere 324 (2023) 138255. https://doi:10.1016/j.chemosphere.2023.138255.

[82] S. Muralimanoharan, C. Li, E.S. Nakayasu, C.P. Casey, T.O. Metz, P.W. Nathanielsz, A. Maloyan, Sexual dimorphism in the fetal cardiac response to maternal nutrient restriction, J. Mol. Cell. Cardiol. 108 (2017) 181–193. https://doi:10.1016/j.yjmcc.2017.06.006.

[83] V. Ramamoorthi Elangovan, N. Saadat, A. Ghnenis, V. Padmanabhan, A.K. Vyas, Developmental programming: adverse sexually dimorphic transcriptional programming of gestational testosterone excess in cardiac left ventricle of fetal sheep, Sci. Rep. 13 (2023) 2682. https://doi:10.1038/s41598-023-29212-9.

[84] L.A. Murtha, M.J. Schuliga, N.S. Mabotuwana, S.A. Hardy, D.W. Waters, J.K. Burgess, D.A. Knight, A.J. Boyle, The processes and mechanisms of cardiac and pulmonary fibrosis, Front. Physiol. 8 (2017) 777. https://doi:10.3389/fphys.2017.00777.

[85] C. Jellis, J. Martin, J. Narula, T.H. Marwick, Assessment of nonischemic myocardial fibrosis, J. Am. Coll. Cardiol. 56 (2010) 89–97. https://doi:10.1016/j.jacc.2010.02.047.

[86] S. Park, S. Ranjbarvaziri, F.D. Lay, P. Zhao, M.J. Miller, J.S. Dhaliwal, A. Huertas-Vazquez, X. Wu, R. Qiao, J.M. Soffer, C. Rau, Y. Wang, H.K.A. Mikkola, A. J. Lusis, R. Ardehali, Genetic regulation of fibroblast activation and proliferation in cardiac fibrosis, Circulation 138 (2018) 1224–1235. https://doi:10.1161/circulationaha.118.035420.

[87] Y. Li, T. Shi, X. Li, H. Sun, X. Xia, X. Ji, J. Zhang, M. Liu, Y. Lin, R. Zhang, Y. Zheng, J. Tang, Inhaled tire-wear microplastic particles induced pulmonary fibrotic injury via epithelial cytoskeleton rearrangement, Environ. Int. 164 (2022) 107257. https://doi:10.1016/j.envint.2022.107257.

[88] S. Basak, M.K. Das, A.K. Duttaroy, Plastics derived endocrine-disrupting compounds and their effects on early development, Birth Defects Res 112 (2020) 1308–1325. https://doi:10.1002/bdr2.1741.

[89] J. Liu, J. Shi, R. Hernandez, X. Li, P. Konchadi, Y. Miyake, Q. Chen, T. Zhou, C. Zhou, Paternal phthalate exposure-elicited offspring metabolic disorders are associated with altered sperm small RNAs in mice, Environ. Int. 172 (2023) 107769. https://doi:10.1016/j.envint.2023.107769.

[90] C. Zhou, L. Gao, J.A. Flaws, Exposure to an environmentally relevant phthalate mixture causes transgenerational effects on female reproduction in mice, Endocrinology 158 (2017) 1739–1754. https://doi:10.1210/en.2017-00100.

[91] M.P. Stern, M. Bartley, R. Duggirala, B. Bradshaw, Birth weight and the metabolic syndrome: thrifty phenotype or thrifty genotype? Diabetes Metab Res Rev 16 (2000) 88–93. https://doi:10.1002/(sici)1520-7560(200003/04)16:2<88::aid-dmrr81>3.0.co;2-m.

[92] X. Wang, Y. Yang, P. Zhu, Y. Wu, Y. Jin, S. Yu, H. Wei, M. Qian, W. Cao, S. Xu, Y. Liu, G. Chen, X. Zhao, Prenatal exposure to diesel exhaust PM(2.5) programmed non-alcoholic fatty liver disease differently in adult male offspring of mice fed normal chow and a high-fat diet, Environ Pollut 255 (2019) 113366. https://doi:10.1016/j.envpol.2019.113366.

[93] Y. Li, M. Xu, Z. Zhang, G. Halimu, Y. Li, Y. Li, W. Gu, B. Zhang, X. Wang, In vitro study on the toxicity of nanoplastics with different charges to murine splenic lymphocytes, J. Hazard Mater. 424 (2022) 127508. https://doi:10.1016/j.jhazmat.2021.127508.

[94] Q. Yang, H. Dai, B. Wang, J. Xu, Y. Zhang, Y. Chen, Q. Ma, F. Xu, H. Cheng, D. Sun, C. Wang, Nanoplastics shape adaptive anticancer immunity in the colon in mice, Nano Lett. 23 (2023) 3516–3523. https://doi:10.1021/acs.nanolett.3c00644.

[95] C. Murano, E. Bergami, G. Liberatori, A. Palumbo, I. Corsi, Interplay between nanoplastics and the immune system of the mediterranean sea urchin paracentrotus lividus, Front. Mar. Sci. 8 (2021) 647394. https://doi:10.3389/fmars.2021.647394.

[96] M. Sendra, A. Saco, M.P. Yeste, A. Romero, B. Novoa, A. Figueras, Nanoplastics: from tissue accumulation to cell translocation into Mytilus galloprovincialis hemocytes. resilience of immune cells exposed to nanoplastics and nanoplastics plus Vibrio splendidus combination, J. Hazard Mater. 388 (2020) 121788. https://doi:10.1016/j.jhazmat.2019.121788.

[97] K. Wang, L. Zhu, L. Rao, L. Zhao, Y. Wang, X. Wu, H. Zheng, X. Liao, Nano- and micro-polystyrene plastics disturb gut microbiota and intestinal immune system in honeybee, Sci. Total Environ. 842 (2022) 156819. https://doi:10.1016/j.scitotenv.2022.156819.

[98] C. Martino, A.H. Dilmore, Z.M. Burcham, J.L. Metcalf, D. Jeste, R. Knight, Microbiota succession throughout life from the cradle to the grave, Nat. Rev. Microbiol. 20 (2022) 707–720. https://doi:10.1038/s41579-022-00768-z.

[99] A. Mishra, G.C. Lai, L.J. Yao, T.T. Aung, N. Shental, A. Rotter-Maskowitz, E. Shepherdson, G.S.N. Singh, R. Pai, A. Shanti, R.M.M. Wong, A. Lee, C. Khyriem, C. A. Dutertre, S. Chakarov, K.G. Srinivasan, N.B. Shadan, X.M. Zhang, S. Khalilnezhad, F. Cottier, A.S.M. Tan, G. Low, P. Chen, Y. Fan, P.X. Hor, A.K.M. Lee, M. Choolani, D. Vermijlen, A. Sharma, G. Fuks, R. Straussman, N. Pavelka, B. Malleret, N. McGovern, S. Albani, J.K.Y. Chan, F. Ginhoux, Microbial exposure during early human development primes fetal immune cells, Cell 184 (2021) 3394–3409.e3320. https://doi:10.1016/j.cell.2021.04.039.

[100] N. Baranzini, L. Pulze, C. Bon, L. Izzo, S. Pragliola, V. Venditto, A. Grimaldi, Hirudo verbana as a freshwater invertebrate model to assess the effects of polypropylene micro and nanoplastics dispersion in freshwater, Fish Shellfish Immunol. 127 (2022) 492–507. https://doi:10.1016/j.fsi.2022.06.043.

[101] K. Kataoka, Y. Tokutomi, E. Yamamoto, T. Nakamura, M. Fukuda, Y.F. Dong, H. Ichijo, H. Ogawa, S. Kim-Mitsuyama, Apoptosis signal-regulating kinase 1 deficiency eliminates cardiovascular injuries induced by high-salt diet, J. Hypertens. 29 (2011) 76–84. https://doi:10.1097/HJH.0b013e32833fc8b0.

[102] M. Kleinewietfeld, A. Manzel, J. Titze, H. Kvakan, N. Yosef, R.A. Linker, D.N. Muller, D.A. Hafler, Sodium chloride drives autoimmune disease by the induction of pathogenic TH17 cells, Nature 496 (2013) 518–522. https://doi:10.1038/nature11868.

[103] I. Vitale, F. Pietrocola, E. Guilbaud, S.A. Aaronson, J.M. Abrams, D. Adam, M. Agostini, P. Agostinis, E.S. Alnemri, L. Altucci, I. Amelio, D.W. Andrews, R. I. Aqeilan, E. Arama, E.H. Baehrecke, S. Balachandran, D. Bano, N.A. Barlev, J. Bartek, N.G. Bazan, C. Becker, F. Bernassola, M.J.M. Bertrand, M.E. Bianchi, M. V. Blagosklonny, J.M. Blander, G. Blandino, K. Blomgren, C. Borner, C.D. Bortner, P. Bove, P. Boya, C. Brenner, P. Broz, T. Brunner, R.B. Damgaard, G.A. Calin, M. Campanella, E. Candi, M. Carbone, D. Carmona-Gutierrez, F. Cecconi, F.K. Chan, G.Q. Chen, Q. Chen, Y.H. Chen, E.H. Cheng, J.E. Chipuk, J.A. Cidlowski, A. Ciechanover, G. Ciliberto, M. Conrad, J.R. Cubillos-Ruiz, P.E. Czabotar, V. D'Angiolella, M. Daugaard, T.M. Dawson, V.L. Dawson, R. De Maria, B. De Strooper, K.M. Debatin, R.J. Deberardinis, A. Degterev, G. Del Sal, M. Deshmukh, F. Di Virgilio, M. Diederich, S.J. Dixon, B.D. Dynlacht, W.S. El-Deiry, J. W. Elrod, K. Engeland, G.M. Fimia, C. Galassi, C. Ganini, A.J. Garcia-Saez, A.D. Garg, C. Garrido, E. Gavathiotis, M. Gerlic, S. Ghosh, D.R. Green, L.A. Greene, H. Gronemeyer, G. Häcker, G. Hajnóczky, J.M. Hardwick, Y. Haupt, S. He, D.M. Heery, M.O. Hengartner, C. Hetz, D.A. Hildeman, H. Ichijo, S. Inoue, M. Jäättelä, A. Janic, B. Joseph, P.J. Jost, T.D. Kanneganti, M. Karin, H. Kashkar, T. Kaufmann, G.L. Kelly, O. Kepp, A. Kimchi, R.N. Kitsis, D.J. Klionsky, R. Kluck, D.V. Krysko, D. Kulms, S. Kumar, S. Lavandero, I.N. Lavrik, J.J. Lemasters, G. Liccardi, A. Linkermann, S.A. Lipton, R.A. Lockshin, C. López-Otín, T. Luedde, M. MacFarlane, F. Madeo, W. Malorni, G. Manic, R. Mantovani, S. Marchi, J.C. Marine, S.J. Martin, J.C. Martinou, P.G. Mastroberardino, J. P. Medema, P. Mehlen, P. Meier, G. Melino, S. Melino, E.A. Miao, U.M. Moll, C. Muñoz-Pinedo, D.J. Murphy, M.V. Niklison-Chirou, F. Novelli, G. Núñez, A. Oberst, D. Ofengeim, J.T. Opferman, M. Oren, M. Pagano, T. Panaretakis, M. Pasparakis, J.M. Penninger, F. Pentimalli, D.M. Pereira, S. Pervaiz, M.E. Peter, P. Pinton, G. Porta, J.H.M. Prehn, H. Puthalakath, G.A. Rabinovich, K. Rajalingam, K.S. Ravichandran, M. Rehm, J.E. Ricci, R. Rizzuto, N. Robinson, C.M. P. Rodrigues, B. Rotblat, C.V. Rothlin, D.C. Rubinsztein, T. Rudel, A. Rufini, K.M. Ryan, K.A. Sarosiek, A. Sawa, E. Sayan, K. Schroder, L. Scorrano, F. Sesti, F. Shao, Y. Shi, G.S. Sica, J. Silke, H.U. Simon, A. Sistigu, A. Stephanou, B.R. Stockwell, F. Strapazzon, A. Strasser, L. Sun, E. Sun, Q. Sun, G. Szabadkai, S.W. G. Tait, D. Tang, N. Tavernarakis, C.M. Troy, B. Turk, N. Urbano, P. Vandenabeele, T. Vanden Berghe, M.G. Vander Heiden, J.L. Vanderluit, A. Verkhratsky, A. Villunger, S. von Karstedt, A.K. Voss, K.H. Vousden, D. Vucic, D. Vuri, E.F. Wagner, H. Walczak, D. Wallach, R. Wang, Y. Wang, A. Weber, W. Wood, T. Yamazaki, H.T. Yang, Z. Zakeri, J.E. Zawacka-Pankau, L. Zhang, H. Zhang, B. Zhivotovsky, W. Zhou, M. Piacentini, G. Kroemer, L. Galluzzi, Apoptotic cell death in disease-Current understanding of the NCCD 2023, Cell Death Differ. 30 (2023) 1097–1154. https://doi:10.1038/s41418-023-01153-w.

[104] Z. Li, S. Zhu, Q. Liu, J. Wei, Y. Jin, X. Wang, L. Zhang, Polystyrene microplastics cause cardiac fibrosis by activating Wnt/β-catenin signaling pathway and promoting cardiomyocyte apoptosis in rats, Environ Pollut 265 (2020) 115025. https://doi:10.1016/j.envpol.2020.115025.

[105] M. Mantri, G.J. Scuderi, R. Abedini-Nassab, M.F.Z. Wang, D. McKellar, H. Shi, B. Grodner, J.T. Butcher, I. De Vlaminck, Spatiotemporal single-cell RNA sequencing of developing chicken hearts identifies interplay between cellular differentiation and morphogenesis, Nat. Commun. 12 (2021) 1771. https://doi:10.1038/s41467-021-21892-z.

[106] Y. Cui, Y. Zheng, X. Liu, L. Yan, X. Fan, J. Yong, Y. Hu, J. Dong, Q. Li, X. Wu, S. Gao, J. Li, L. Wen, J. Qiao, F. Tang, Single-cell transcriptome analysis maps the developmental track of the human heart, Cell Rep. 26 (2019) 1934–1950.e1935. https://doi:10.1016/j.celrep.2019.01.079.